1998

Characterizing elevation effects of a prolate spheroidal HRTF model

Richard W. Novy
San Jose State University

Follow this and additional works at: https://scholarworks.sjsu.edu/etd_theses

INFORMATION TO USERS

CHARACTERIZING ELEVATION EFFECTS OF A PROLATE SPHEROIDAL HRTF
MODEL

A Thesis

Presented to

The Faculty of the Department of General Engineering

San Jose State University

In Partial Fulfillment

of the Requirements for the Degree

Master of Science

by

Richard W. Novy

May 1998

UMI Number: 1389669

Copyright 1998 by
Novy, Richard W.

UMI
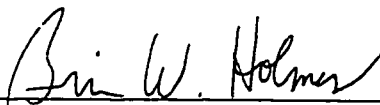
APPROVED FOR THE DEPARTMENT OF GENERAL ENGINEERING

_____

Dr. Richard O. Duda, Thesis Advisor

_____

Dr. Brian W. Holmes

_____
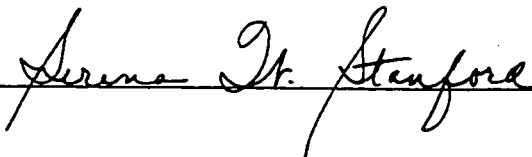
Dr. Walter J. Utz, Jr.   (M. HAMBABA)
                                (SIGNING FOR
                                  DR. WALTER UTZ)

APPROVED FOR THE UNIVERSITY

_____

ABSTRACT

CHARACTERIZING ELEVATION EFFECTS OF A PROLATE SPHEROIDAL HRTF MODEL

by Richard W. Novy

The scattering of an acoustic, monochromatic plane wave from a prolate spheroidal human head is investigated to determine if incorporating this shape into the human head-related transfer function (HRTF) could add the ability to model elevation effects. Scattering is characterized for a prolate spheroid with length-to-width ratio of roughly 2.5:1, and the results are compared with those from a sphere of diameter equal to the major axis of the spheroid. Results are presented in the form of surface plots for five different frequencies. Also discussed is the prolate spheroidal wave function, an example of solving the Fourier coefficients involved in their generation, and some comments on extending the HRTF using a triaxial ellipsoid.

ACKNOWLEDGMENTS

No man works in a vacuum, and I am no exception. A work of this magnitude is never accomplished alone. Of the multitude of people who helped, several deserve a special mention.

For helping a complete stranger struggling with prolate spheroidal wave functions, and for generosity with his time and effort, Dr. Thomas B. A. Senior of the University of Michigan Radiation Laboratory has my deepest appreciation. This thesis simply would not have been possible without his help.

For helping a complete stranger on the other side of the world, I want to thank Tatyana Levitina. Although most of her efforts eventually went unused for this thesis, hopefully the inclusion of Appendix A will help the next researcher locate the wonderfully well written papers by Ms. Levitina and her colleagues.

For helping me up when I was down, and supporting this effort, Dearl Moore.

To my thesis committee, Dr. Richard O. Duda, Dr. Brian W. Holmes, and the late Dr. Walter J. Utz, Jr., who all were a great help to more than just the thesis.

I started this degree without any children, and finish it with three. For all her help with the kids, I thank my mother-in-law, Rosalina Atok.

To Russell, Reanna, and Audrey: you are my inspiration. Reach for the stars, and let nothing get in your way. Strength comes from within. The only person who can hold you down forever is you, and the only person who can make your dreams come true is you. You can, and I know that some day you will.

Most of all, I thank the love of my life, Rica. Without your support and encouragement, this thesis wouldn't have happened. I dedicate this thesis to you and our family.

Table of Contents

List of Figures

List of Symbols

a=Radius of spherical head model.

$c = \frac{1}{2}kd$; Used as a representation of frequency.

d=interfocal distance

d_r^{mn} =Fourier coefficient for the series expansion of prolate spheroidal wave functions.

ε_m=The Neumann Symbol; ε_m =1 when m=0, ε_m =2 for other positive integers.

φ =Prolate spheroidal coordinate defining angle about the z-axis a point lies in.

η=Prolate spheroidal coordinate defining which hyperboloid a point lies on.

HRTF=Head Related Transfer Function.

$h_n^{(1)\prime}$ =first derivative of the spherical Hankel function of the first kind.

$j_m(c\xi)$=Spherical Bessel function of the first kind, argument $c\xi$.

k=wavenumber

ℓ_{2k}^{mn} =coefficients in the expansion of $\lambda_{mn}(c)$, with k the summation index.

$\lambda_{mn}(c)$=Eigenvalues used in the expansion of the coefficients d_r^{mn} .

P_n^m =Associated Legendre function of the first kind.

Q_n^m =Associated Legendre function of the second kind.

$R_{mn}^{(k)}(c,\xi)$ =Radial spheroidal wave function of the kth kind.

$S_{mn}^{(k)}(c,\eta)$ =Angular spheroidal wave function of the kth kind.

V_i=Velocity potential of the incident wave.

V_s=Velocity potential of the scattered wave.

ξ=Prolate spheroidal coordinate defining which ellipsoid a point lies on.

ξ_1=Rigid ellipsoid of interest in the prolate spheroidal coordinate system.

$y_m(c\xi)$= Spherical Bessel function of the second kind, argument $c\xi$.

ζ=elevation angle, measured from the positive z-axis.

Introduction

One of the main reasons that the audio portion of virtual reality lags behind the video is that the interaction of a sound wave with the human head is very complicated. Humans hear in three dimensions. Stereo is a clumsy attempt at three dimensional sound. When listening through headphones, people perceive the sounds to be emanating from inside the head. Simple mathematical models have been constructed to synthesize three-dimensional sound, and some perform reasonably well, but none is convincing enough to use in virtual reality applications. The most difficult part of the problem is creating a head-related transfer function which convincingly reproduces mathematically what the human head does to a sound wave in physical reality.

The human head-related transfer function, hereafter referred to as HRTF, captures the physical clues that people use to locate sound sources. This transfer function defines how sound is converted from a wave in free space into a pressure at the ear. It is affected by head shape, body shape, pinna shape, and many other factors. The human HRTF is far too complicated to model exactly, but reasonable models for it can be constructed by using basic acoustic principles. Even if simple models are insufficient for applications, they provide valuable insight to help in understanding experimentally measured HRTF responses.

In an HRTF model, the head is represented by a simple shape in the appropriate coordinate system, and an acoustic wave is scattered by the model head. Pressure is then

sampled on the model head at the location of the ear. Considerable work has been done on the HRTF by Duda and Martens using a spherical model head [Duda and Martens 1997]. Their model provides insight to the azimuthal and range effects of the HRTF. This work was continued by combining it with a pinna model, then successfully using the results to synthesize binaural sound with coarse elevation effects [Brown 1996].

The elevation effects in the aforementioned work rely only on a model of the human pinna. Due to its symmetry, a spherical head can only provide information for one angular dimension. Azimuth was the dimension chosen for a number of reasons, including the fact that a real head is more circular in azimuth. In order to gain some understanding of the elevation effects caused by head shape on the response of the HRTF, the head model must move away from spherical symmetry. Another shape, such as a prolate spheroid, or a triaxial ellipsoid, must be used in order to produce these effects. This solution is deceptively simple. The mathematics involved in using either the prolate spheroidal or the ellipsoidal coordinate systems is far more complicated than that involved in spherical coordinates. The solution to the three-dimensional Helmholz equation in either of these coordinate systems is also much more computationally intensive.

The work for this thesis began with the intention of using a triaxial ellipsoid to model the human head. Some progress was made, but this approach was abandoned due to time constraints. Some comments and references for using the triaxial ellipsoid appear in Appendix A.

With the triaxial ellipsoid eliminated, work began on modeling the HRTF using a prolate spheroid. Building on published material on acoustic scattering by simple shapes [Bowman, Senior, and Uslenghi 1987], a model HRTF was constructed using MATLAB.® This model was based on plane wave diffraction by a prolate spheroid. Due to various difficulties which will be discussed in greater detail, an exaggerated major-to-minor axis ratio of roughly 2.5 to 1 was used in this model.

There has been at least one other published work using a prolate spheroidal model HRTF [Sugiyama 1989], but it is written in Japanese. At the time this manuscript was written, no English translation was available. Although their work does not parallel this thesis, their equations and figures are consistent with those used here.

The elevation results presented here are interesting. At low frequencies, it appears that the spherical model and the spheroidal models have similar responses. When frequencies increase, the responses are very different. These results will be discussed in some detail in chapter five. The incorporation of the results into a fully functional HRTF model, simulating sound with elevation effects, is well out of the scope of this project.

These results are very preliminary, and, as such, are limited in their applicability to the HRTF. More work with the functions in question is required before a prolate spheroidal model can reasonably be used for synthesis of binaural sound. Still, these results, with their exaggerated head elongation, provide some insight to the acoustics due to breaking the spherical symmetry, and will hopefully encourage others to continue along this path.

1.0 <u>Existing Models</u>

The most studied model for the human HRTF uses a spherical head. Despite its unrealistic shape, the ease of working with this model is a great convenience due to its simple geometry. In many cases, the spherical model is quite adequate to describe the behavior of the HRTF. This is particularly true of the coarse, low-frequency behavior, and of behavior that is limited to the equatorial plane.

The main limitation to the spherical model is due to its symmetry, which manifests itself as an inability to recognize elevation differences in sound sources. A so-called "cone of confusion" is introduced. For a sound incident the ear at some angle θ away from perpendicular, there is a cone with vertex of angle 2θ at the ear, from whence the sound might have its source. That is why this model is generally used without elevation effects. Even this limitation is somewhat abated when the spherical model is combined with current models of the human pinna. Together with the pinna model, the spherical head is quite adequate to allow simulation of binaural sounds which can be localized to within about thirty degrees of elevation [Brown 1996].
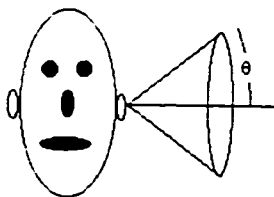
Figure 1.1 - The cone of confusion.

Duda and Martens have extensively researched the response of the HRTF for a spherical head model. Their findings demonstrate that computational results using the spherical model compare quite favorably with the overall pattern of measurements made with the so-called KEMAR dummy, particularly at low frequencies. Both exhibit a six decibel gain at high frequencies for signals with low angle of incidence to the ear. Both exhibit the characteristic "bright spot" at incident angles approaching 180 degrees away from the ear. Finally, at high frequencies, both exhibit a distinct roll-off at large angles (Fig. 1.2).
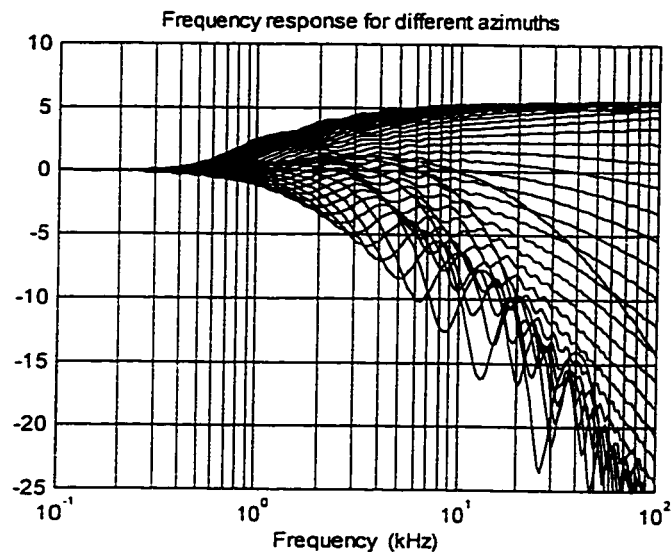
Figure 1.2 - Plot of frequency response of the spherical HRTF model from the work of Duda and Martens. Frequency is plotted along the x-axis, and decibels along the y-axis. Each line represents a different angle of incidence. Plots representing sounds directly or nearly directly incident the ear are toward the top of the plot. As angle increases, the plots move toward the bottom of the graph. Sounds incident exactly opposite the ear are represented by the arc through the middle of the plot. This arc is evidence that this model produces the traditional bright spot due to constructive interference. Note the 6 dB gain at higher frequencies for small incident angles, and the roll-off at larger angles. Figure courtesy of Richard O. Duda.

Clearly, the work by Duda and Martens is a strong foundation on which to build a model for the HRTF which incorporates a more realistic response. Of particular interest is improvement of elevation localization when the pinna model is incorporated. There is no question that the pinna is important for elevation effects in the HRTF, but it appears to provide only very coarse ability to locate sound sources in elevation. There are two other obvious features humans use to assist in locating sounds in elevation: the head is not a sphere, and sound reflects from the shoulders.

This thesis is a first attempt to characterize whether the head shape plays much of a role in the HRTF. It does not attempt to incorporate a non-spherical head into a full-blown HRTF model. It does, however, examine the amplitude of the sound at the location of one ear on a prolate spheroid model head for a plane wave incident from all directions.

This is the second known work for which a prolate spheroid is considered as the basis for an HRTF. The first work appeared in the *Journal of the Acoustical Society of Japan* [Sugiyama 1989]. At the time this manuscript was written, no English translation of the work was available. Figure captions are in English, and they compare spherical, prolate spheroidal, and KEMAR measurements for inter-aural length and cross-correlation coefficients in a reverberating room. Their equations are consistent with those used in this work, but their study appears to be quite different. An English translation should be a priority for anyone continuing this research.

2.0 Solution to the Helmholz Equation in Prolate Spheroidal Coordinates

In order to allow a reasonable chance of successfully modeling the human HRTF, the shape used to model the head is extremely important. The main criterion which influences the selection of head shape is separability of the Helmholz equation in three dimensions. The head-shape must lie upon a surface formed by setting one of the variables to a constant. For example, the most commonly used shape for the HRTF is the sphere, formed by setting the range variable to a constant in spherical coordinates.

The specification of one sphere to act as the head greatly simplifies the mathematics involved when spherical coordinates are used. Selection of the same sphere in the Cartesian coordinate system would complicate the mathematics involved. For that reason, using a coordinate system where the head shape occurs naturally is convenient.

Because human heads are generally roundish, most of the eleven separable coordinate systems [Morse and Feshbach 1953] are inappropriate for HRTF models. The only four that remain as reasonable choices are the spherical, prolate spheroidal, oblate spheroidal, and triaxial ellipsoidal coordinate systems. Of these, the oblate spheroidal coordinate system can immediately be discarded since it does not really resemble the human head. The use of the spherical HRTF model was discussed in chapter one, and its limitations are the motivation for this thesis. The remaining two coordinate systems are the obvious choices for a more robust HRTF to include elevation effects. Of these two, the prolate spheroidal coordinate system is far simpler.

Work for this thesis began with the "nothing ventured, nothing gained" attitude, by attempting to model the HRTF using triaxial ellipsoidal coordinates. The work was making progress, but was abandoned due to time constraints. A brief discussion of ellipsoidal coordinates, and references to important papers on the subject, are contained in Appendix A.

Although using a prolate spheroid to model the human head did nothing to eliminate idealizations due to the inherent azimuthal symmetry, insight was clearly gained over spherical coordinates. The question of whether azimuthal asymmetry impacts the HRTF, however, remains unanswered.

Since the prolate spheroidal coordinate system is not commonly used, and many people are completely unfamiliar with it, a discussion of the coordinate system will precede the discussion of separation of variables in it. The most widely cited work in English language research appears to be [Flammer 1957], and it is his notation that is used throughout this thesis. A more readily available resource, featuring a mostly adequate summary of prolate spheroidal coordinates and the spheroidal wave function-- the solution to the Helmholz equation in this coordinate system--is available in [Abramowitz and Stegun 1972]. The material presented here is based upon their summary in chapter 21, and all equations may be found there.

The prolate spheroidal coordinate system is formed by rotating the two-dimensional elliptical coordinate system about the major axis of the ellipses. The prolate

spheroidal coordinate system is a family of confocal prolate spheroids and hyperboloids

of revolution (Fig. 2.1). The rotated elliptical coordinates are

$$\xi = \frac{r_1 + r_2}{2f}, \quad \eta = \frac{r_1 - r_2}{2f},$$

(2.1)

where r_1 and r_2 are the distances from a given point to each focus of the confocal ellipses

and hyperbolas, and $2f$ is the interfocal distance. Upon revolving the coordinate system

about the major axis of the ellipses, three coordinates emerge: ξ, η, and φ. Flammer

orients the ellipsoids resulting from this revolution in such a way that the major axes lie

along the Cartesian z-axis. For any given point (ξ, η, φ), the spheroid containing the point

is given by ξ, the hyperboloid by η, and the angle about the axis of revolution by φ.

The range of ξ is $[1, \infty)$, where $\xi = 1$ represents the degenerate ellipsoid forming a

line segment joining the foci, and $\xi = \infty$ is an infinitely large sphere (such that the distance

$2f$ can be considered zero). The range of η is $[-1, 1]$, where $\eta = -1, +1$ are degenerate

hyperboloids forming rays along the negative and positive z-axes, respectively. The value

$\eta = 0$ is the degenerate hyperboloid forming the xy-plane. The range of φ is $[0, 2\pi)$,

measured as an angle around the axis of rotation.
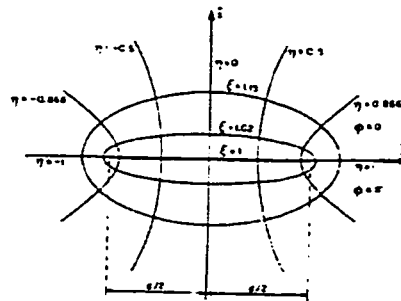
Figure 2.1 - The prolate spheroidal geometry [Bowman, Senior, and Uslenghi 1987]. Figure appears by permission of Taylor and Francis, Inc.

The Cartesian coordinates (x,y,z) relate to the prolate spheroidal coordinates (ξ,η,φ) by the following relations:

$$x = \frac{1}{2}d\sqrt{(\xi^2 - 1)(1 - \eta^2)}\cos\varphi, \qquad (2.2a)$$

$$y = \frac{1}{2}d\sqrt{(\xi^2 - 1)(1 - \eta^2)}\sin\varphi, \qquad (2.2b)$$

$$z = \frac{1}{2}d\xi\eta, \qquad (2.2c)$$

where d is the distance between the foci. It is clear from the form of these expressions that it is far simpler to convert from prolate spheroidal coordinates to Cartesian than in the other direction.

In spheroidal coordinates, the Wave Equation takes the form

$$(\nabla^2 + k^2)\Phi = \frac{\partial}{\partial\xi}\left[(\xi^2 - 1)\frac{\partial\Phi}{\partial\xi}\right] + \frac{\partial}{\partial\eta}\left[(1 - \eta^2)\frac{\partial\Phi}{\partial\eta}\right] + \frac{(\xi^2 - \eta^2)}{(\xi^2 - 1)(1 - \eta^2)}\frac{\partial^2\Phi}{\partial\varphi^2} + c^2(\xi^2 - \eta^2)\Phi = 0. \quad (2.4)$$

where $c = \dfrac{kd}{2}$, the product of the semi-focal distance and the wavenumber [Bowman, Senior, and Uslenghi 1987]. The variable c is used as a way to represent frequency in the literature, and should not be confused with the speed of sound. It is worth noting that equation (2.4) can be converted to the oblate spheroidal coordinate system by simply replacing ξ by $i\xi$, and c by $-ic$ [Flammer 1957].

If the angular solution to the wave equation is represented by $S_{mn}(c,\eta)$, and the radial by $R_{mn}(c,\xi)$, then the function Φ can be written in the separable form

$$\Phi = R_{mn}(c,\xi)S_{mn}(c,\eta) \, {}^{\cos}_{\sin} \, m\varphi. \qquad (2.5)$$

$R_{mn}(c,\xi)$ and $S_{mn}(c,\eta)$ are the solution to the same ordinary differential equation over different ranges of the independent variable (recall the ranges of ζ and η):

$$\frac{d}{d\xi}\left[(\xi^2-1)\frac{d}{d\xi}R_{mn}(c,\xi)\right]-\left(\lambda_{mn}-c^2\xi^2+\frac{m^2}{\xi^2-1}\right)R_{mn}(c,\xi)=0 \qquad (2.6)$$

and

$$\frac{d}{d\eta}\left[(1-\eta^2)\frac{d}{d\eta}S_{mn}(c,\eta)\right]+\left(\lambda_{mn}-c^2\eta^2-\frac{m^2}{1-\eta^2}\right)S_{mn}(c,\eta)=0. \qquad (2.7)$$

The quantity λ_{mn} is both separation constant and eigenvalue, determined such that the value of $R_{mn}(c,\xi)$ is finite at $\xi=\pm1$, and $S_{mn}(c,\eta)$ is finite at $\eta=\pm1$. The solutions to these two equations are discussed in more detail in the next chapter.

3.0 Prolate Spheroidal Wave Functions

3.1 The Prolate Angular Function

The solutions to equations (2.6) and (2.7) are the prolate spheroidal angular and radial wave functions. The solutions have some similarities, but the differences are very strong, due mainly to the boundary conditions. Each type will be discussed separately. The material presented here is due to Flammer.

The angular solution, $S_{mn}(c,\eta)$, actually takes two forms. Both are defined as Fourier expansions in associated Legendre functions. The prolate angular function of the first kind is defined as

$$S_{mn}^{(1)}(c, \eta) = \sum_{r=0,1}^{\infty}{}' d_r^{mn}(c) P_{m+r}^m(\eta).\qquad(3.1)$$

The prolate angular function of the second kind is defined as

$$S_{mn}^{(2)}(c, \eta) = \sum_{r=-\infty}^{\infty}{}' d_r^{mn}(c) Q_{m+r}^m(\eta),\qquad(3.2)$$

where, in both cases, d_r^{mn} is the Fourier coefficient, and the prime above the summation sign indicates that it includes only even values of r when $(n-m)$ is even, and odd values of r when $(n-m)$ is odd. P_n^m refers to the associated Legendre function of the first kind, and Q_n^m to the associated Legendre function of the second kind. The angular spheroidal wave function of the second kind is not considered part of the solution to the Helmholz equation because it is singular at $\eta = \pm 1$. For that reason, it

will not be further discussed. Henceforth, $S_{mn}(c,\eta)$ will implicitly refer only to the prolate angular function of the first kind.

Presented below are drawings of the first few angle functions, generated by MATLAB® code for the angle function, S. These plots make use of coefficients d_0^{mn} (or d_1^{mn}) though d_8^{mn} (or d_9^{mn}), which is the extent the series were expanded for all work presented in this thesis.
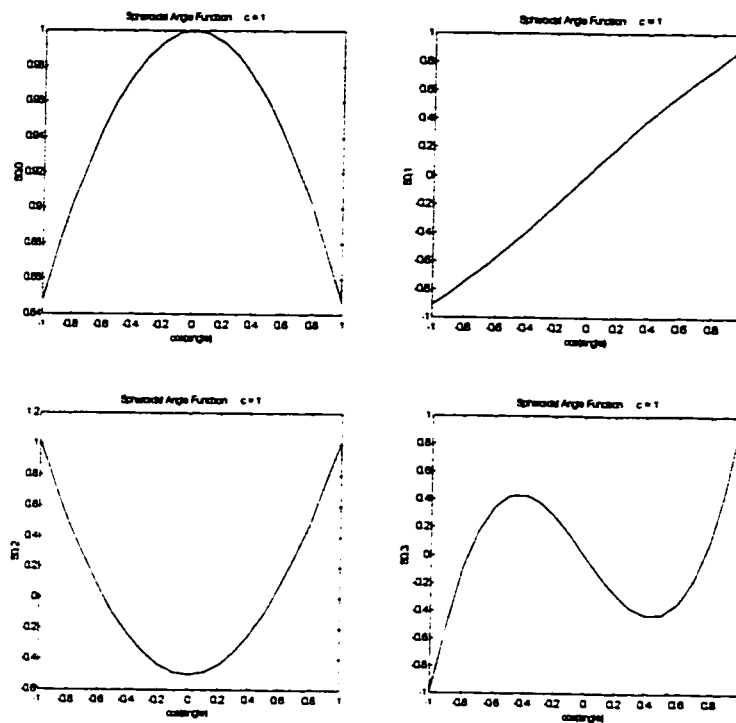
Figure 3.1: Angular Spheroidal Wave Functions. Upper left, m=0, n=0. Upper right, m=1, n=1. Lower left, m=1, n=2. Lower right, m=1, n=3. The variable m is the degree, and n the order, of the angular spheroidal wave function.

The main difficulty in working with the angular spheroidal function is the generation of the coefficients d_r^{mn}. This is not a difficulty that is easy to overcome. There is no analytic representation for the d_r^{mn} coefficients. Instead, they must be

represented by series expansions in c^2, which must be generated individually, because there is no formula for this, either. Upon studying the material presented later in this section, it becomes clear that there is no obvious way to generate these series computationally. As mentioned earlier, the independent variable, c, is the product of half the interfocal length of the spheroid, and the wavenumber of the incoming acoustic signal. It is used as the representation of frequency in these expressions.

There is no aesthetic way to present the recursions and normalizations involved in the derivation of these coefficients. Both Flammer and Abramowitz and Stegun are unclear in communicating the generation of the series representations of these coefficients, so this material will be followed by an example with comments. Flammer presents the following equations with some explanation in the text, whereas Abramowitz and Stegun essentially present the material in the form of a list without explanation. Both books also furnish a great deal of material not included here, and Flammer, in particular, discusses convergence requirements of some continued fractions involved in generation of these relations. In fact, the material presented here is limited to a practical minimum. The interested reader should refer to Flammer if more depth is required. This material should be sufficient to allow—with perhaps considerable work—generation of any coefficient desired.

The coefficients d_r^{mn} subscribe to the following recursion relation due to Flammer:

$$\frac{(2m+r+2)(2m+r+1)c^2}{(2m+2r+3)(2m+2r+5)}d_{r+2}^{mn}(c)$$

$$+ \quad \left[(m+r)(m+r+1)-\lambda_{mn}(c)+\frac{2(m+r)(m+r+1)-2m^2-1}{(2m+2r-1)(2m+2r+3)}c^2\right]d_r^{mn}(c)$$

$$+ \quad \frac{r(r-1)c^2}{(2m+2r-3)(2m+2r-1)}d_{r-2}^{mn}(c)=0, \quad (r \geq 0). \tag{3.3}$$

This is a second-order difference equation with two non-trivial solutions, only one of which converges. The solution of interest is, of course, the converging one, where the ratio d_r^{mn}/d_{r-2}^{mn} approaches zero as $-c^2/(4r^2)$. With that condition enforced, equation (3.1) is absolutely convergent for all finite η.

The eigenvalues of a transcendental equation relating two continued fractions, developed by Flammer, are important to the construction of the d_r^{mn} coefficients. The transcendental equation itself is not directly used, so it is not presented here. The eigenvalues are in the form of a power series—also in c^2. Algebraic manipulation of the continued fraction representation of the eigenvalues, described in Flammer, yields the following expressions, allowing easy calculation of the first five terms in the series representation of the eigenvalues. Flammer lists a sixth term which is omitted here for the sake of space. The desired eigenvalues have the form

$$\lambda_{mn}(c) = \sum_k \ell_{2k}^{mn}c^{2k}, \tag{3.4}$$

and the first five coefficients are expanded below.

$$\ell_0^{mn} = n(n+1) \tag{3.5}$$

$$\ell_2^{mn} = \tfrac{1}{2}\left[1 - \frac{(2m-1)(2m+1)}{(2n-1)(2n+3)}\right] \tag{3.6}$$

$$\ell_4^{mn} = \tfrac{1}{2}\left[\frac{(n-m-1)(n-m)(n+m-1)(n+m)}{(2n-3)(2n-1)^3(2n+1)}\right.$$

$$\left. - \frac{(n-m+1)(n-m+2)(n+m+1)(n+m+2)}{(2n+1)(2n+3)^3(2n+5)}\right] \tag{3.7}$$

$$\ell_6^{mn} = \left(4m^2-1\right)\left[\frac{(n-m+1)(n-m+2)(n+m+1)(n+m+2)}{(2n-1)(2n+1)(2n-3)^5(2n+5)(2n+7)}\right.$$

$$\left. - \frac{(n-m-1)(n-m)(n+m-1)(n+m)}{(2n-5)(2n-3)(2n-1)^5(2n+1)(2n+3)}\right] \tag{3.8}$$

$$\ell_8^{mn} = 2\left(4m^2-1\right)^2 A + \tfrac{1}{16}B + \tfrac{1}{8}C + \tfrac{1}{2}D \tag{3.9}$$

$$A = \frac{(n-m-1)(n-m)(n+m-1)(n+m)}{(2n-5)^2(2n-3)(2n-1)^7(2n+1)(2n+3)^2}$$

$$- \frac{(n-m+1)(n-m+2)(n+m+1)(n+m+2)}{(2n-1)^2(2n+1)(2n+3)^7(2n+5)(2n+7)^2} \tag{3.10}$$

$$B = \frac{(n-m-3)(n-m-2)(n-m-1)(n-m)(n+m-3)(n+m-2)(n+m-1)(n+m)}{(2n-7)(2n-5)^2(2n-3)^3(2n-1)^4(2n+1)}$$

$$- \frac{(n-m+1)(n-m+2)(n-m+3)(n-m+4)(n+m+1)(n+m+2)(n+m+3)(n+m+4)}{(2n+1)(2n+3)^4(2n+5)^3(2n+7)^2(2n+9)}$$

$$\tag{3.11}$$

17

$$C = \frac{(n-m+1)^2(n-m+2)^2(n+m+1)^2(n+m+2)^2}{(2n+1)^2(2n+3)^7(2n+5)^2}$$

$$- \frac{(n-m-1)^2(n-m)^2(n+m-1)^2(n+m)^2}{(2n-3)^2(2n-1)^7(2n+1)^2} \tag{3.12}$$

$$D = \frac{(n-m-1)(n-m)(n-m+1)(n-m+2)(n+m-1)(n+m)(n+m+1)(n+m+2)}{(2n-3)(2n-1)^4(2n+1)^2(2n+3)^4(2n+5)}$$

$$\tag{3.13}$$

The ℓ_8^{mn} term is in the form Abramowitz and Stegun provide. Flammer depicts it fully expanded as one long expression.

The above is adequate to determine the coefficients d_r^{mn} to within an arbitrary factor of d_0^{mn}. In order to completely determine all the coefficients, a normalization scheme must be employed. There are three schemes outlined in Abramowitz and Stegun, including Flammer's. One more is presented by Morse and Feshbach, who use far different notation, and somewhat different methods to address the prolate spheroidal wave functions. The normalization scheme of choice is Flammer's, and that is the one presented here. Flammer's relations are:

$$\sum_{r=0}^{\infty}{}' \frac{(-1)^{\frac{r}{2}}(r+2m)!}{2^r(\frac{r}{2})!(\frac{r+2m}{2})!} d_r^{mn} = \frac{(-1)^{\frac{n-m}{2}}(n+m)!}{2^{n-m}(\frac{n-m}{2})!(\frac{n+m}{2})!}, \quad \text{(n-m) even,} \tag{3.14a}$$

$$\sum_{r=1}^{\infty}{}' \frac{(-1)^{\frac{r-1}{2}}(r+2m+1)!}{2^r(\frac{r-1}{2})!(\frac{r+2m+1}{2})!} d_r^{mn} = \frac{(-1)^{\frac{n-m-1}{2}}(n+m+1)!}{2^{n-m}(\frac{n-m-1}{2})!(\frac{n+m+1}{2})!}, \quad \text{(n-m) odd.} \tag{3.14b}$$

Again, the prime above the summation sign indicates the that only even terms are used in (3.14a), and odd terms in (3.14b).

Expanding the coefficients d_r^{mn} is where both Flammer, and Abramowitz and Stegun are unclear. To a person who is not constantly working with this type of expression, the approach to take in solving for the appropriate coefficients for any given d_r^{mn} is really not very obvious. For this reason, the determination of d_0^{00} is provided as an example. Upon studying this example, it should be clear how to proceed in generating any d_r^{mn} desired. Hopefully, the inclusion of this example will make work with spheroidal wave functions accessible to more people. The computations for this example were graciously provided by Dr. Thomas B. A. Senior of the University of Michigan Radiation Laboratory, in an unpublished correspondence [Senior 1998]. In fact, without Professor Senior's generous assistance, the majority of this chapter would not have been written. A 1960 paper by Senior, appearing in the *Canadian Journal of Physics*, presents the series expansion produced by this example, and that for six other coefficients [Senior 1960].

For d_r^{mn} in this example, m and n are set to zero. Begin by entering zeros in the appropriate places in equation (3.3). This reduces the recursion relation to

$$\frac{(r+2)(r+1)c^2}{(2r+3)(2r+5)}d_{r+2}^{00}(c) + \left[r(r+1) - \lambda_{00}(c) + \frac{2r(r+1)-1}{(2r-1)(2r+3)}c^2 \right]d_r^{00}(c)$$

$$+ \quad \frac{r(r-1)c^2}{(2r-3)(2r-1)}d_{r-2}^{00}(c) = 0 . \qquad (3.15)$$

It is also necessary to determine the series for $\lambda_{00}(c)$ from equation (3.4), by setting m and n to zero in equations (3.5) through (3.13). Upon doing that, the resulting series is

$$\lambda_{00}(c) = \tfrac{1}{3}c^2 + \tfrac{2}{135}c^4 - \tfrac{4}{8505}c^6 + \gamma c^8 + ..., \qquad (3.16)$$

where $\gamma = \frac{182}{3^7 \cdot 7^2 \cdot 5^3}$. (Notation is Senior's.)

When r is set to zero in equation (3.15), the recursion reduces to

$$\tfrac{2}{15}c^2 d_2^{00} = \left(\lambda_{00}(c) - \tfrac{1}{3}c^2\right)d_0^{00}. \qquad (3.17)$$

By substituting equation (3.16) into (3.17), the resulting recursion is in place as

$$d_2^{00} = \left[\tfrac{1}{9}c^2 - \tfrac{2}{567}c^4 + \tfrac{1358}{18}c^6 + ...\right]d_0^{00}. \qquad (3.18)$$

Next, the normalization scheme must be simplified by entering zeros for m and n. Because m and n are both zero, $(n-m)$ is even, so equation (3.14a) is the correct expression to use. Upon entering zeros in the appropriate places, this reduces to

$$\sum_{r=0}^{\infty}{}' \frac{(-1)^{\frac{r}{2}} r!}{2^r \left(\frac{r}{2}\right)! \left(\frac{r}{2}\right)!} d_r^{00} = 1. \qquad (3.19)$$

Expanding this series yields

$$d_0^{00} - \tfrac{1}{2}d_2^{00} + \tfrac{3}{8}d_4^{00} - \tfrac{5}{16}d_6^{00} + ... = 1. \qquad (3.20)$$

The normalization expansion in equation (3.20) is the key to finding the expansion for d_0^{00}. Since the d_r^{mn} coefficients will be represented in series expansions, they can be written as:

$$d_0^{00} = A_0 + A_1 c^2 + A_2 c^4 + A_3 c^6 + ..., \qquad (3.21)$$

$$d_2^{00} = B_1 c^2 + B_2 c^4 + B_3 c^6 + \dots, \tag{3.22}$$

and

$$d_4^{00} = C_2 c^4 + C_3 c^6 + \dots \tag{3.23}$$

When writing these expansions, it is critical to remember that the expansion begins with the c term having the same exponent as the subscript on d. Substituting equations (3.21) through (3.23) into equation (3.20), and equating coefficients shows that

$$A_0 = 1, \tag{3.25}$$

$$A_1 - \tfrac{1}{2} B_1 = 0, \tag{3.26}$$

and

$$A_2 - \tfrac{1}{2} B_2 + \tfrac{3}{8} C_2 = 0. \tag{3.27}$$

With some manipulation, equation (3.18) can be written as

$$d_2^{00} = -\tfrac{1}{9} \left\{ 1 - \tfrac{2}{63} c^2 - \tfrac{135\gamma}{2} c^4 - \dots \right\} d_0^{00} c^2. \tag{3.28}$$

Upon substituting the expansions in equations (3.21) and (3.22), this becomes

$$B_1 + B_2 c^2 + B_3 c^4 + \dots = -\tfrac{1}{9} \left\{ 1 - \tfrac{2}{63} c^2 - \tfrac{135\gamma}{2} c^4 - \dots \right\} \left\{ A_0 + A_1 c^2 + A_2 c^4 + \dots \right\}. \tag{3.29}$$

Once again, equating coefficients reveals that

$$B_1 = -\tfrac{1}{9} A_0 = -\tfrac{1}{9}. \tag{3.30}$$

Using this result with (3.25) makes it clear that

$$A_1 = -\tfrac{1}{18}. \tag{3.31}$$

It is also not difficult to show that

$$B_2 = -\tfrac{1}{9}\left(A_1 - \tfrac{2}{63}\right) = \tfrac{11}{1134}\,,$$
(3.32)

and that

$$B_3 = -\tfrac{1}{9}\left(A_2 - \tfrac{2}{63}A_1 - \tfrac{135\gamma}{2}\right).$$
(3.33)

With some manipulation,

$$9B_3 + A_2 = \tfrac{2}{63}A_1 + \tfrac{135\gamma}{2} = -\tfrac{1}{9^2 \cdot 7} + \tfrac{135\gamma}{2}\,,$$
(3.34)

which shall be referred to shortly.

In order to arrive at the A_2 term, some additional work is required. Substituting $r = 2$ into equation (3.3) yields the recursion

$$d_0^{00} + \tfrac{2}{7}d_4^{00} + \left\{9 + \tfrac{3}{2}\lambda_{00} + \tfrac{11}{14}c^2\right\}\frac{d_2^{00}}{c^2} = 0.$$
(3.35)

Upon replacing $\lambda_{00}(c)$ with its expansion, this develops into

$$d_0^{00} + \tfrac{2}{7}d_4^{00} + \left\{9 + \tfrac{2}{7}c^2 + \tfrac{1}{45}c^4 + \ldots\right\}\frac{d_2^{00}}{c^2} = 0.$$
(3.36)

Once again, substituting the expansion forms of the d_r^{mn} terms (equations 3.21 - 3.23), and equating coefficients, produces relations which allow determination of A_2. In particular, the relation

$$A_2 + 9B_3 + \tfrac{2}{7}B_2 + \tfrac{1}{45}B_1 + \tfrac{2}{7}C_2 = 0\,,$$
(3.37)

in concert with equation (3.34), produces

$$-\tfrac{1}{3^4 \cdot 7} + \tfrac{135\gamma}{2} + \tfrac{2}{7}C_2 + \tfrac{11}{3^4 \cdot 7^2} - \tfrac{1}{3^4 \cdot 5} = 0\,,$$
(3.38)

so,

$$C_2 = \tfrac{1}{525}. \tag{3.39}$$

Equation (3.27) can now be solved for A_2, yielding

$$A_2 = \tfrac{67}{16200}. \tag{3.40}$$

Putting the terms together finally produces the series representation for d_0^{00}, which is

$$d_0^{00} = 1 - \tfrac{1}{18}c^2 + \tfrac{67}{16200}c^4 + O\!\left(c^6\right). \tag{3.41}$$

As mentioned above, Senior has expanded several other series through the number of terms that can be achieved without further expansion of $\lambda_{00}(c)$.

3.2 The Prolate Radial Function

Like the angle functions, there are two solutions to the radial portion of the wave equation in prolate spheroidal coordinates. Unlike the angle functions, neither solution can be discarded in a cavalier manner, as both solutions can be forced to fit the boundary conditions. Additionally, under Neumann conditions (rigid spheroid), the first derivative of the radial functions are used in place of the function itself. The condition at infinity is the Somerfeld Radiation Condition. Discussion of the Somerfeld Radiation Condition is out of the scope of this thesis, and it is taken on faith that this condition is met.

In addition to the two solutions mentioned above, two linear combinations of the solutions exist in much the same way that Bessell Functions combine to create

Hankel functions. This relationship is more than a similarity. In fact, the spherical Bessel and spherical Hankel functions are both degenerate forms of the radial prolate spheroidal wave functions, in the limit as the interfocal distance approaches zero. The form of these functions is described below.

The *radial spheroidal wave function of the first kind* is an expansion in spherical Bessel functions of the first kind:

$$R_{mn}^{(1)}(c,\xi) = \frac{1}{\displaystyle\sum_{r=0,1}^{\infty}{}' d_r^{mn}(c)\frac{(2m+r)!}{r!}} \left(\frac{\xi^2-1}{\xi^2}\right)^{\frac{1}{2}m} \sum_{r=0,1}^{\infty}{}' i^{r+m-n} d_r^{mn}(c)\frac{(2m+r)!}{r!} j_{m-r}(c\xi),$$

(3.42)

where the summation in the denominator is a scaling factor. The *radial spheroidal wave function of the second kind* is similar, but is an expansion in spherical Bessel functions of the second kind:

$$R_{mn}^{(2)}(c,\xi) = \frac{1}{\displaystyle\sum_{r=0,1}^{\infty}{}' d_r^{mn}(c)\frac{(2m+r)!}{r!}} \left(\frac{\xi^2-1}{\xi^2}\right)^{\frac{1}{2}m} \sum_{r=0,1}^{\infty}{}' i^{r+m-n} d_r^{mn}(c)\frac{(2m+r)!}{r!} y_{m+r}(c\xi).$$

(3.43)

The radial spheroidal wave functions of the third and fourth kinds are defined as:

$$R_{mn}^{(3),(4)}(c,\xi) = R_{mn}^{(1)}(c,\xi) \pm iR_{mn}^{(2)}(c,\xi).$$

(3.44)

Flammer describes $R_{mn}^{(2)}(c,\xi)$ as converging very slowly, perhaps only in the limit. Of course, this is also true of $R_{mn}^{(3)}(c,\xi)$ and $R_{mn}^{(4)}(c,\xi)$. Because these expressions

converge slowly, it becomes quite computationally intensive to calculate specific values in the radial direction, including at the surface of the prolate spheroid of interest. This is one reason why a lookup table approach was used for the radial functions. Further discussion of the lookup table appears in a later chapter, but because a lookup table was used, no plots of the radial function were generated in conjunction with this thesis.

4.0 Construction of the HRTF Models

The traditional definition of the HRTF is the ratio of the pressure at the ear with the free-field pressure at the origin. Rather than working with pressure, the acoustics literature prefers to work with velocity potential $V(\mathbf{x},t)$. Pressure is retrieved from the velocity potential by the following expression [Morse and Feshbach 1953]:

$$p - p_o = -\frac{\partial V}{\partial t} - \gamma V,$$ (4.1)

where p_0 is the ambient pressure, and γ is a damping coefficient (and should not be confused with γ in the previous chapter). The velocity potential at the ear is defined as $V_i + V_s|_{\bar{x}=\xi_1}$, where V_i is the incident wave, and V_s is the scattered wave. The velocity potential at the origin is defined as $V_i|_{\bar{x}=0}$. The HRTF is the ratio of the two:

$$HRTF = \frac{V_i + V_s \big|_{\bar{x}=\xi_1}}{V_i \big|_{\bar{x}=0}}.$$ (4.2)

Here, the nomenclature $\bar{x} = \xi_1$ should be interpreted as representing the surface of the head model, i.e., the sphere or prolate spheroid of interest, in its appropriate coordinate system. Because the waves are propagating in a medium with negligible viscosity (air), γ is set to 0, so damping is neglected. The time dependence has the form $e^{(i\omega t)}$, thus it is separable from the rest of the expression. Upon taking the partial derivative of V with

respect to time to achieve the representation for pressure, most of the expression is treated as a constant, and a factor of $i\omega t$—with a density constant δ_o if not normalized away—is produced. The extra constants, as well as the time dependence, cancel upon taking the ratio described above. Working with pressure or velocity potential is, therefore, equivalent when modeling the response of the HRTF.

4.1 Spherical HRTF Model

Investigation into the response, at the location of the human ear, of a plane wave scattered by a prolate spheroidal model head would be meaningless without first preparing a benchmark. The commonly used spherical-head model is the ideal place to begin the investigation, as it will provide a reference against which to gauge the response of the prolate spheroid. The approach used here developed quite differently from that of Duda and Martens, but the results are consistent.

The spherical model described below is based on the material appearing in chapter 10 of [Bowman, Senior, and Uslenghi 1987], and that material is discussed in far greater detail in that book. Familiarity with the spherical coordinate system is assumed.

Recall that the denominator of the HRTF is $V_i|_{\bar{r}=0}$. In spherical coordinates, the form of this expression is

$$V_i = \exp\left\{ikr\left[\cos\theta_o\cos\theta + \sin\theta_o\sin\theta\cos(\varphi-\varphi_o)\right]\right\}\Big|_{r=0}. \qquad (4.3)$$

With r set to 0, $V_i=1$. The denominator of the HRTF being unity greatly simplifies the expressions, and the HRTF becomes simply V_i+V_s at the surface of the sphere. The expression, when $r = a$, is

$$HRTF = V_i + V_s = \frac{i}{(ka)^2}\sum_{n=0}^{\infty}(-i)^n(2n+1)\frac{P_n(\cos\theta)}{h_n^{(1)\prime}(ka)}. \qquad (4.4)$$

Note that in the denominator, the first derivative of the spherical Hankel function appears, in order to meet the acoustically hard boundary conditions.

A test to verify this model is describing the same behavior as that described by Duda and Martens, so one of their plots was duplicated using the relations described in Bowman, Senior, and Uslenghi. The original plot, produced by the author, using Duda and Martens' original MATLAB® code, appeared as Figure (1.2). The reproduction, using equation (4.4), appears below.
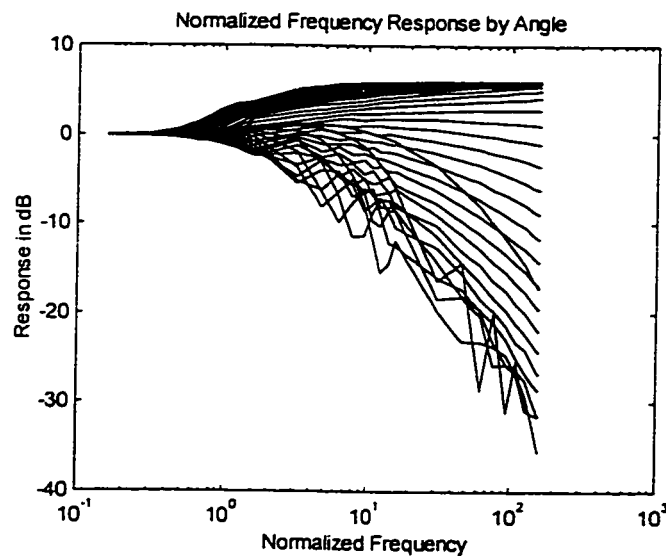

Figure 4.1 - Plot of frequency response from spherical head model of the HRTF using the methods developed for this thesis. Compare with the plot in figure (1.2). Jagged lines in the plot are due to aliasing caused by insufficient sample points at high frequencies. Normalized frequency is c.

There are several notable features of the two plots which merit discussion. The code developed by Duda and Martens will generate figure (1.2) in roughly five minutes on a computer equipped with a 200 MHz CPU. The code developed for this thesis took roughly seven *hours* to plot the same graph. There is one main reason for this. Duda and Martens spent a great deal of effort developing and exploiting recursions to eliminate redundant calculations. For this thesis, the Legendre and Hankel functions were generated from scratch for each term in equation (4.4), amounting to over 250 terms for the highest of frequencies. That the algorithm used in figure (4.1) was intended as a verification of this HRTF model, and was not intended to be used as a research tool, made a seven-hour run tolerable for one execution of the code. Duda and Martens' spherical HRTF algorithm is clearly the more efficient by orders of magnitude.

Most of the seven-hour processing time was taken up by extending the number of terms used in series (4.4) for higher frequencies. A self-adjusting algorithm was used to increase the number of terms in equation (4.4) as a function of ka, itself a function of frequency. A plot created while developing this algorithm, (Fig 4.2), demonstrates how crucial an adequate number of terms can be for this type of model. Figure (4.2) was generated using the number of terms for all frequencies that figure (4.1) used for the very lowest of frequencies. Figure (4.2) was generated in under 20 minutes, using the same brute-force methods of figure (4.1), other than using fewer terms.
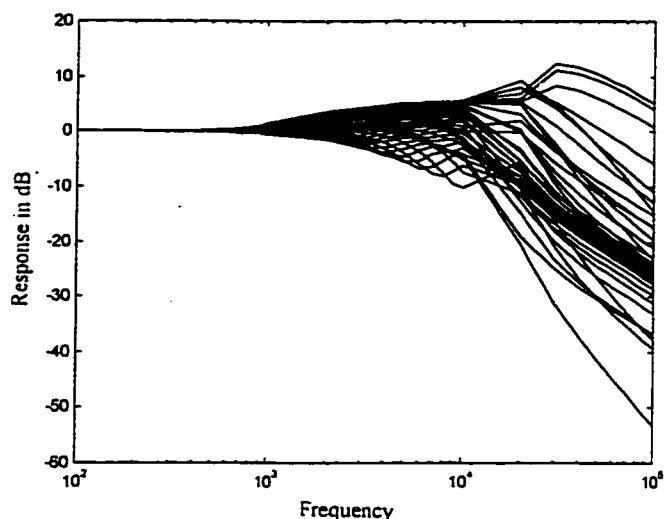
Figure 4.2 - This plot demonstrates how critical a sufficient number of terms can be. This is the same plot as in figure (4.1) with two major differences. First, the frequency axis is not normalized, and second, the number of terms was too small for the higher frequencies. The model holds through about 10^4 then it fails completely. The point of failure would be near 10^1 if the plot were normalized.

An additional interesting feature of figure (4.1) is the jaggedness of the plot in the higher frequency range. This is a result of the limited number of samples used for calculating the curves. Only ten samples were used per decade. This small number of terms is sufficient to verify that the overall performance of the model is the same as the Duda-Martens model, but insufficient to prevent aliasing at the higher frequencies.

4.2 Prolate Spheroidal HRTF Model

The prolate spheroidal HRTF model is based on the work presented in chapter 11 of [Bowman, Senior, and Uslenghi 1987]. It is a mathematical model of a plane wave incident upon an acoustically rigid prolate spheroid.

The plane wave is incident at an angle ζ, measured from the positive z-axis. A plane wave incident at the angle ζ has (dimensionless) velocity potential

$$V_i = \exp\{ik(x\sin\zeta + z\cos\zeta)\}. \qquad (4.5)$$

At the origin, $V_i = 1$. Once again, the denominator of the HRTF ratio presented in equation (4.2) is unity. As with the spherical case, the HRTF is equivalent to looking at $V_i + V_s$ at the surface of the spheroid. In the prolate case, this expression is

$$V_i + V_s = \frac{2}{c(\xi_1^2 - 1)} \sum_{m=0}^{\infty} \sum_{n=m}^{\infty} \varepsilon_m \frac{i^{n+1}}{N_{mn}} \frac{1}{R_{mn}^{(3)'}(c,\xi_1)} S_{mn}(c,\cos\xi) S_{mn}(c,\eta)\cos m\varphi, \qquad (4.6)$$

where ε_m is the Neumann Symbol ($\varepsilon_m = 1$ when $m = 0$, and $\varepsilon_m = 2$ when m is another positive integer). Note that the first derivative of the radial prolate function appears in the denominator due to the Neumann boundary condition imposed at the spheroid.

4.3 MATLAB® Implementation

Creating a MATLAB® algorithm to calculate the HRTF response for a plane wave incident the spherical head from any given angle is quite straightforward. In order to keep this model consistent with how the prolate model was developed, the incident wave needed to have its direction specified by an elevation and azimuth angle. The main difficulty was converting these two angles into the single angle required by equation (4.4). The solution to this problem proved to be a simple application of the law of
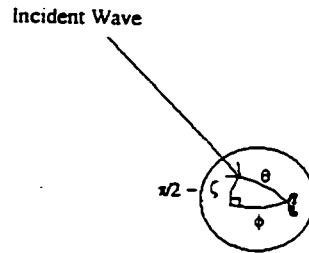
Figure 4.3 - Azimuth angle φ and elevation angle π/2 - ζ are converted to one angle q by use of the law of cosines for spherical triangles.

cosines for spherical triangles [Spiegel 1968]. Due to the geometry used for the problem, the triangle in question is always a right triangle, which simplifies the expression used for this angle conversion to

$$\theta = \arccos\left[\cos\varphi\cos\left(\tfrac{\pi}{2}-\zeta\right)\right]. \tag{4.7}$$

The angle θ in equation (4.7) is inserted in the Legendre polynomial of equation (4.4). The Legendre polynomial is generated using the MATLAB® function Legendre, keeping only the $m = 0$ terms. The derivative of the spherical Hankel function is constructed by generating the derivatives of the spherical Bessel functions of the first and second kind, then adding them per the definition of the spherical Hankel function,

$$h^{(1)\prime}(z) = j'(z) + iy'(z). \tag{4.8}$$

The spherical functions are constructed per their definitions, using the MATLAB® functions besselj and bessely. The rest of the calculation is simply an exercise in summing a finite series.

Creating an algorithm for the prolate model HRTF proved to be much more challenging. Because understanding of the generation of the coefficients d_r^{mn} was achieved very late, a look-up table approach was forced on the project. For the derivative of the radial function, a look-up table proved invaluable. Whenever one of these values was required, the MATLAB® code retrieved it from a table rather than generating the value. The roundest spheroid for which tabulated coefficients [Flammer 1957] were available was $\xi_1 = 1.077$, defining a prolate spheroid with length-to-width ratio of roughly $2\frac{1}{2}:1$. It was this restriction on ξ_1 that forced this study to be limited to the plane wave case, representing an acoustic point source at infinity. The ability to generate other coefficients d_r^{mn} allows study of range effects because ζ is then a variable that can be worked with.

There were two main look-up tables used, both based on tabulated values appearing in [Flammer 1957]. For the prolate angle functions, the coefficients d_r^{mn} were looked up, then the angle functions calculated for any angular resolution desired. This is possible because the angle function only depends on the d_r^{mn} specific to the surface of interest.

For the radial portion of the acoustic equation, the derivative of the radial function was looked up. The reasons for this were the unwieldy form of the derivative, and the slow convergence of the prolate radial function of the second kind. Sufficient accuracy for the radial function would have been very expensive in terms of computation time.

Also, looking up the radial portion allowed the terms to be calculated in one table reference for d_r^{mn} instead of many. Since resolution in range was not an issue, it was preferable to use the efficiency of the direct table reference. All other terms in equation (4.6) are generated on the fly, and a simple summation of a double finite series ties all the pieces together. A copy of all MATLAB® code can be found in the Appendix B, and the look-up tables in Appendix C.

5.0 Results

5.1 Comments on HRTF Models and Presentation of Results

The simulations run with the spherical and prolate spheroidal HRTF models were identical save for the acoustically rigid head-shape. A plane wave of a pure acoustic tone was incident the surface from different directions. The wave started from the direction of the positive z-axis. An elevation angle ζ is defined as the angle between the positive z-axis and the direction the plane wave is arriving from. In other words, it is measured from the vertical, rather than from the horizontal, which is normally thought of when elevation is discussed (Fig. 5.1). The angle ζ was incremented in 5 degree steps, from 0 to 90 degrees. For each angle ζ, the azimuth, φ, was varied from 0 to 180 degrees, also in 5 degree steps. An angle $\varphi = 180$ is directly incident the ear, whereas an angle of $\varphi = 0$ is incident on the other side of the head, where the other ear would be located.

In the first step of ζ, the plane wave is incident the very top of the head. Since there is no elevation component to the direction of incidence, there is no effect as φ changes. The wave is simply pivots around the z-axis. Once $\zeta > 0$, azimuthal effects begin to appear, and as ζ grows, these effects become more pronounced (Figure 5.1).

The frequency of the incident wave was limited by available values for d_r^{mn}, which were determined via tables included in [Flammer 1957]. This, in turn, limited the values for c. The variable c is related to the wave number and semi-focal distance by

$$c = \tfrac{1}{2}kd. \qquad\qquad (5.1)$$
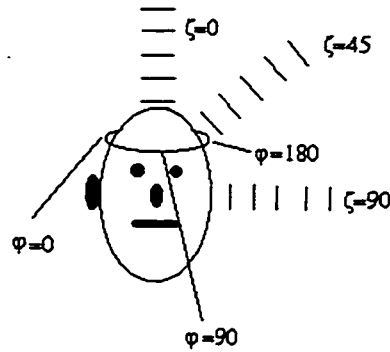
Figure 5.1 - Geometry of the incident plane waves.

For this thesis, c was limited to the integers 1,2,3,4, and 5. This corresponds to frequencies of $f_1 = 530$ Hz, $f_2 = 1060$ Hz, $f_3 = 1590$ Hz, $f_4 = 2120$ Hz, and $f_5 = 2650$ Hz, and wavelengths of 65 cm, 32 cm, 22 cm, 16 cm, and 13 cm, respectively. Fortunately, all of these frequencies fall into the region of (Figure 4.2) with sufficient terms for convergence. This allowed the fast algorithm, with relatively few terms in c, to be used in the spherical HRTF model. The MATLAB® routine for the spherical model runs to completion in under seven minutes on a computer equipped with 200 MHz CPU. In contrast, the routine for the prolate spheroid model takes about a hour, even with the lookup tables.

Because the spheroidal model was restricted to prolate spheroids for which Flammer included tables, the selection of head shapes was very limited. Flammer's tables

were taken from earlier works using the prolate spheroid to model a wire in antenna theory. As unintuitive as it might be, the standard way to refer to a specific spheroidal surface is by its ξ coordinate, and the spheroid of interest is noted as ξ_1. The relationship between ξ_1 and length-to-width ratio of the prolate spheroid is

$$\frac{length}{width} = \frac{\xi_1}{\sqrt{\xi_1^2 - 1}}. \qquad (6.2)$$

The roundest spheroid with a preconstructed list of coefficients and values available in [Flammer 1957] is $\xi_1 = 1.077$. This translates to length-to-width ratio of 2.69:1. In order to be consistent with [Sugiyama 1989], the height of the model head is fixed at 22.2 cm. The fact that $\xi_1 = 1.077$ forces the width of the model head to 8.25 cm; not a particularly convincing head shape. Despite the obvious drawbacks to exaggerating the eccentricity, in many ways it is more useful than a realistic head shape. The differences between the spherical and prolate spheroidal head models are greatly magnified, and the effects of going out-of-round are more evident.

The results with the spherical model are rather subtle, and are presented in several plots below. The azimuth angle, φ, is plotted along the right side of the diagram, and the elevation angle, ζ, is plotted along the left side—both are in degrees. The plots on the left half of the page have amplitude plotted along the z-axis, normalized in the sense that the incident wave is unity. The plots on the right half of the page are similar to those on the left except the z-axis is plotted in decibels. Results from the top of the head are located along the right-front edge. Results from the wave directly incident the ear is located at

the back-right corner of the plot. The characteristic "bright spot," resulting when the wave is incident the side of the head opposite the ear, is seen at the back-left corner of the plot. The "bright-spot" effect is due to constructive interference of the scattered acoustic waves, traveling around the head in each direction and meeting at the opposite side. Note that the frequencies used are in the low and moderate ranges for the spherical model when the transition from low to high is defined as a signal with wavelength equal to the circumference of the sphere. For the prolate spheroidal model, some interesting effects appear when $c = 4$ and $c = 5$. Two very-high-frequency plots, using the spherical model, are also presented for comparison to these. Below each surface plot appears the same plot looking at the elevation-amplitude plane or elevation-decibel plane, respectively. This allows a more accurate measure of the peaks and troughs of the response surfaces. MATLAB® was allowed to auto-scale the z-axis because much of the detail is lost when the scales are fixed. Fixed z-axis plots appear at the end of this chapter.

In order to demonstrate the higher-frequency characteristics of the response of the spherical HRTF, plots have been generated for $c = 20$, and $c = 40$. Clearly, the high-frequency characteristics of the spherical model HRTF differ from those of the spheroidal HRTF.

Frequency and sphere radius are coupled, so increasing frequency while holding the radius constant has the same effect as increasing the radius while holding the frequency constant. The sphere used in these simulations had a 22.2 cm diameter, which

is the same size as the major-axis of the prolate spheroid. There are some obvious

features which are strikingly different between the two HRTF models.

Figure 5.2 - Response of a 530 Hz plane wave incident a spherical head model. Raw amplitude is shown in the left plot, and decibels in the right. Elevation is plotted along the left edge, and azimuth along the right edge. The ear is located at 90 degrees elevation, and at 180 degrees azimuth (the back corner).

Figure 5.3 - Response of a 530 Hz plane wave incident a spherical head model. These plots are the same as those appearing in figure 5.2 except only the elevation effects are seen.

Figure 5.4 - Response of a 1060 Hz plane wave incident a spherical head model. Raw amplitude is shown in the left plot, and decibels in the right. Elevation is plotted along the left edge, and azimuth along the right edge. The ear is located at 90 degrees elevation, and at 180 degrees azimuth (the back corner).

Figure 5.5 - Response of a 1060 Hz plane wave incident a spherical head model. These plots are the same as those appearing in figure 5.4 except only the elevation effects are seen.
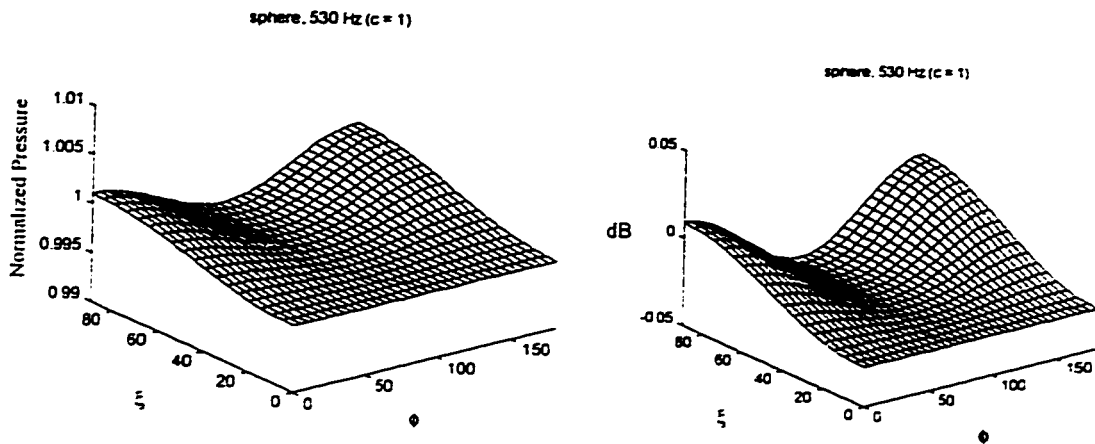
sphere. 1590 Hz (c = 3) sphere. 1590 Hz (c = 3)

Figure 5.6 - Response of a 1590 Hz plane wave incident a spherical head model. Raw amplitude is shown in the left plot, and decibels in the right. Elevation is plotted along the left edge, and azimuth along the right edge. The ear is located at 90 degrees elevation, and at 180 degrees azimuth (the back corner).

sphere. 1590 Hz (c = 3) sphere. 1590 Hz (c = 3)

Figure 5.7 - Response of a 1590 Hz plane wave incident a spherical head model. These plots are the same as those appearing in figure 5.6 except only the elevation effects are seen.

sphere. 2120 Hz (c = 4)

sphere. 2120 Hz (c = 4)

Figure 5.8 - Response of a 2120 Hz plane wave incident a spherical head model. Raw amplitude is shown in the left plot, and decibels in the right. Elevation is plotted along the left edge, and azimuth along the right edge. The ear is located at 90 degrees elevation, and at 180 degrees azimuth (the back corner).
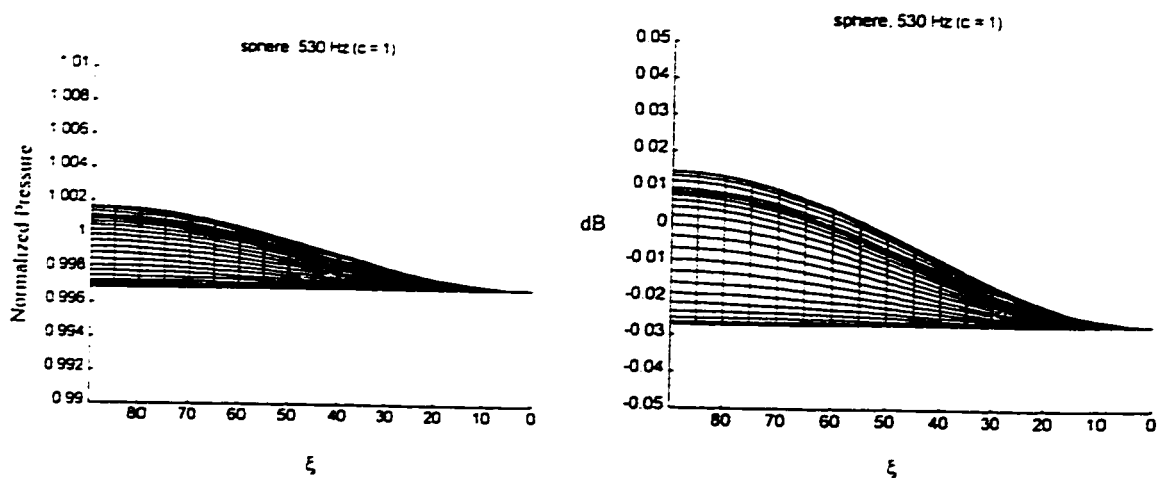
sphere. 2120 Hz (c = 4)

sphere. 2120 Hz (c = 4)

Figure 5.9 - Response of a 2120 Hz plane wave incident a spherical head model. These plots are the same as those appearing in figure 5.8 except only the elevation effects are seen.
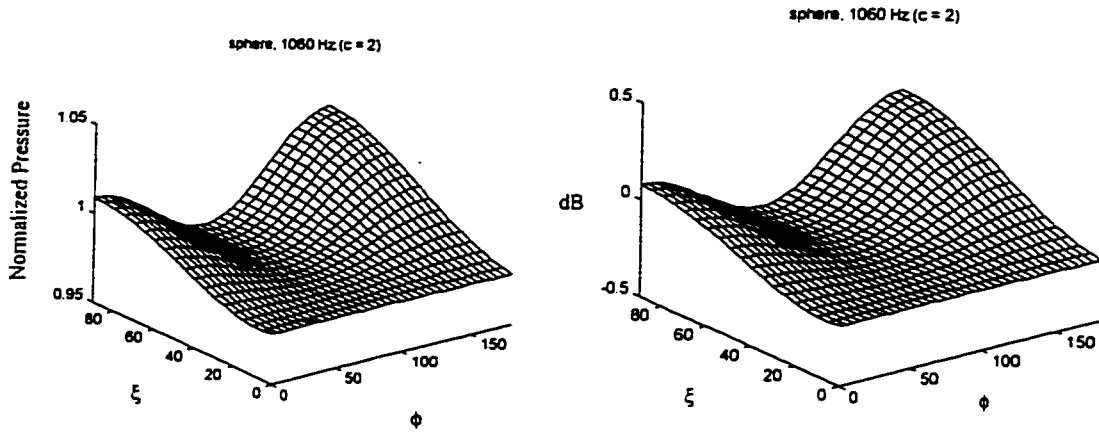
sphere. 2650 Hz (c = 5)

sphere. 2650 Hz (c = 5)

Figure 5.10 - Response of a 2650 Hz plane wave incident a spherical head model. Raw amplitude is shown in the left plot, and decibels in the right. Elevation is plotted along the left edge, and azimuth along the right edge. The ear is located at 90 degrees elevation, and at 180 degrees azimuth (the back corner).
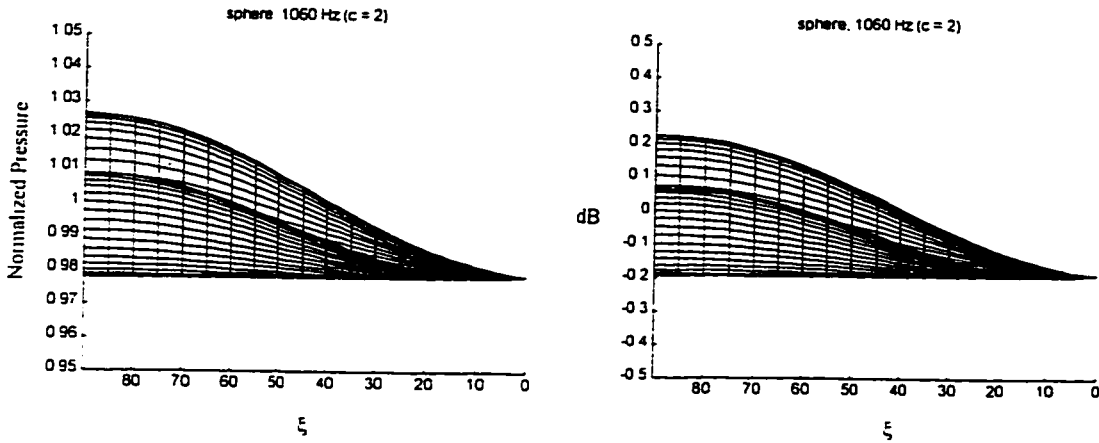

sphere. 2650 Hz (c = 5)

sphere. 2650 Hz (c = 5)

Figure 5.11 - Response of a 2650 Hz plane wave incident a spherical head model. These plots are the same as those appearing in figure 5.10 except only the elevation effects are seen.
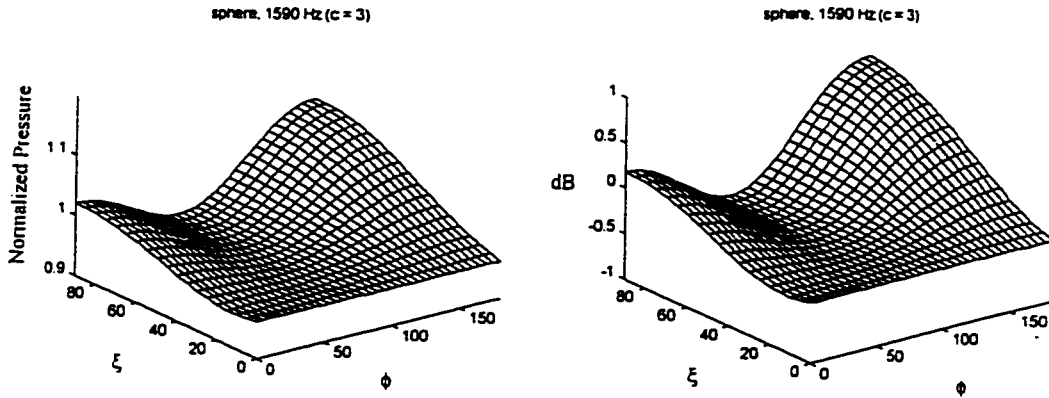
Figure 5.12 - Response of a 10600 Hz plane wave incident a spherical head model. Raw amplitude is shown in the left plot, and decibels in the right. Elevation is plotted along the left edge, and azimuth along the right edge. The ear is located at 90 degrees elevation, and at 180 degrees azimuth (the back corner).
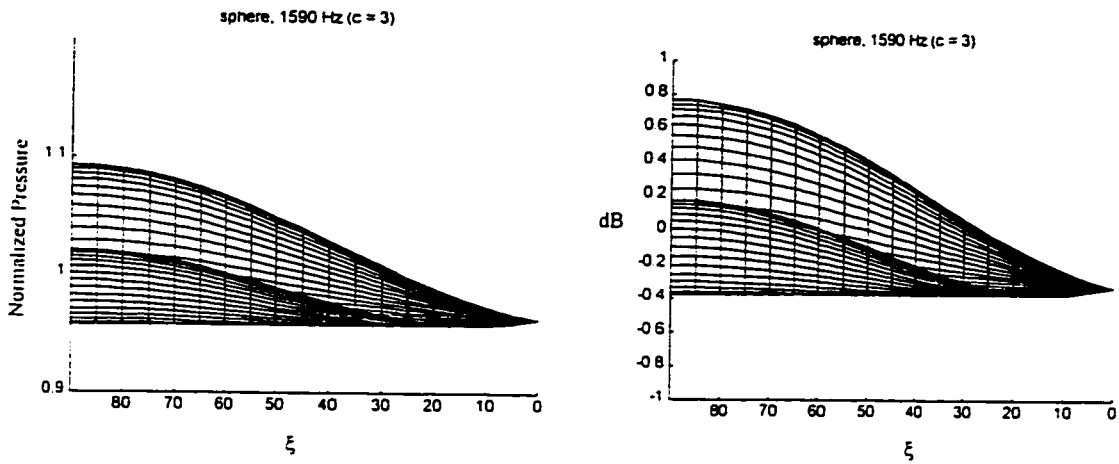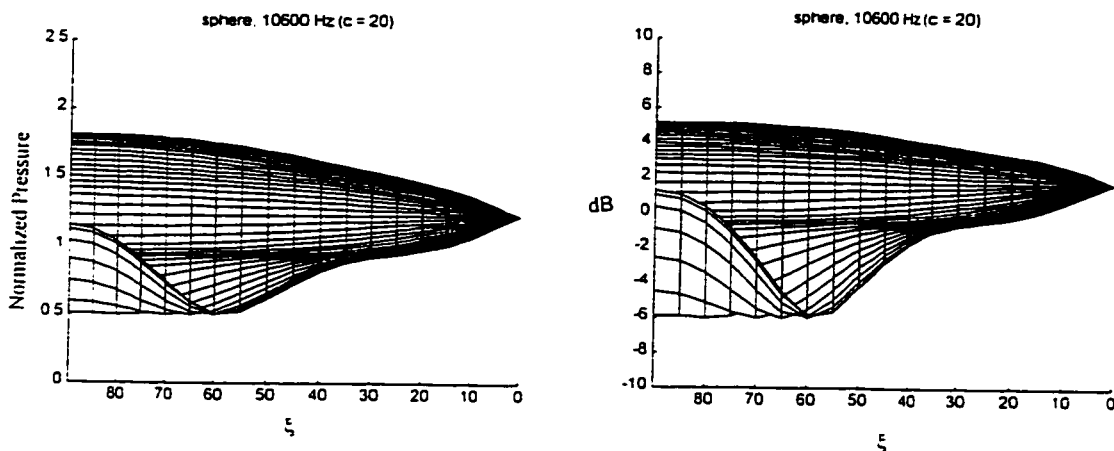

Figure 5.13 - Response of a 10600 Hz plane wave incident a spherical head model. These plots are the same as those appearing in figure 5.12 except only the elevation effects are seen.
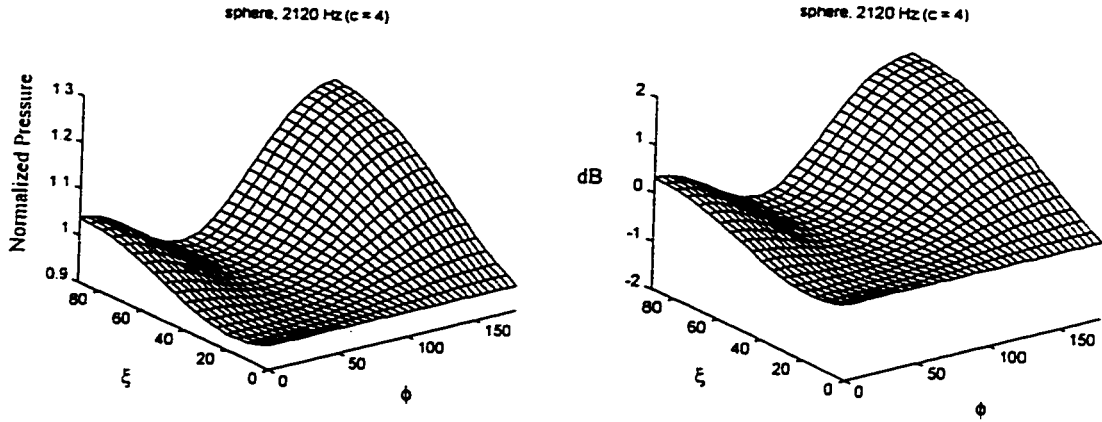
sphere, 21200 Hz (c = 40)

sphere, 21200 Hz (c = 40)

Figure 5.14 - Response of a 21200 Hz plane wave incident a spherical head model. Raw amplitude is shown in the left plot, and decibels in the right. Elevation is plotted along the left edge, and azimuth along the right edge. The ear is located at 90 degrees elevation, and at 180 degrees azimuth (the back corner).

sphere, 21200 Hz (c = 40)

sphere, 21200 Hz (c = 40)

Figure 5.15 - Response of a 21200 Hz plane wave incident a spherical head model. These plots are the same as those appearing in figure 5.14 except only the elevation effects are seen.

Figure 5.16 - Response of a 530 Hz plane wave incident a prolate spheroidal head model. Raw amplitude is shown in the left plot, and decibels in the right. Elevation is plotted along the left edge, and azimuth along the right edge. The ear is located at 90 degrees elevation, and at 180 degrees azimuth (the back corner).
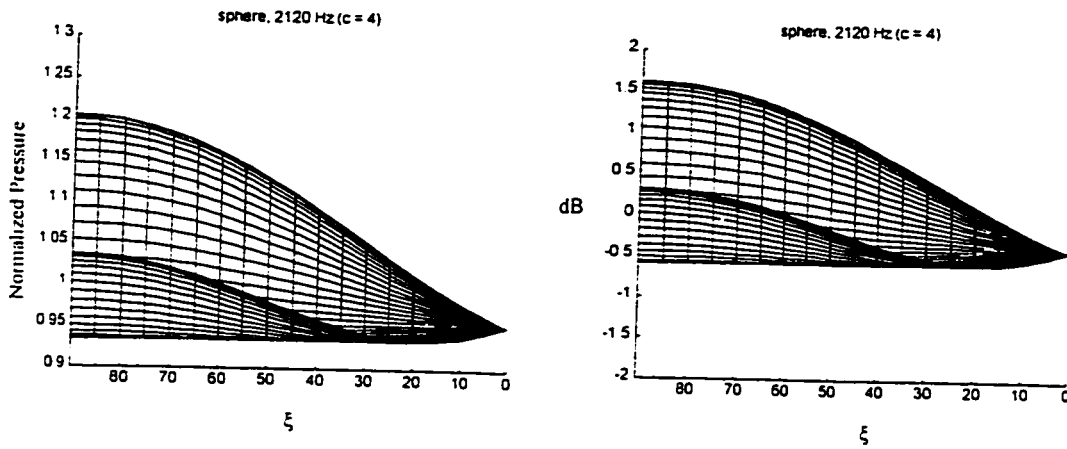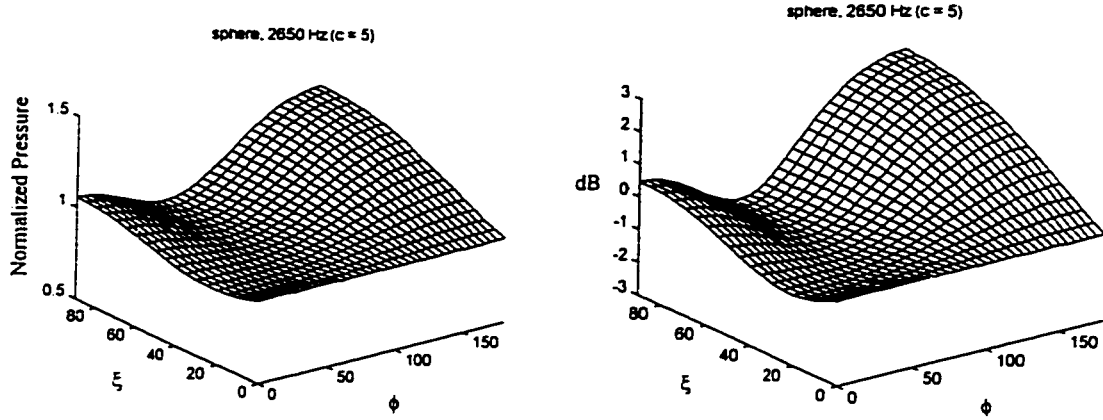

Figure 5.17 - Response of a 530 Hz plane wave incident a prolate spheroidal head model. These plots are the same as those appearing in figure 5.16 except only the elevation effects are seen.
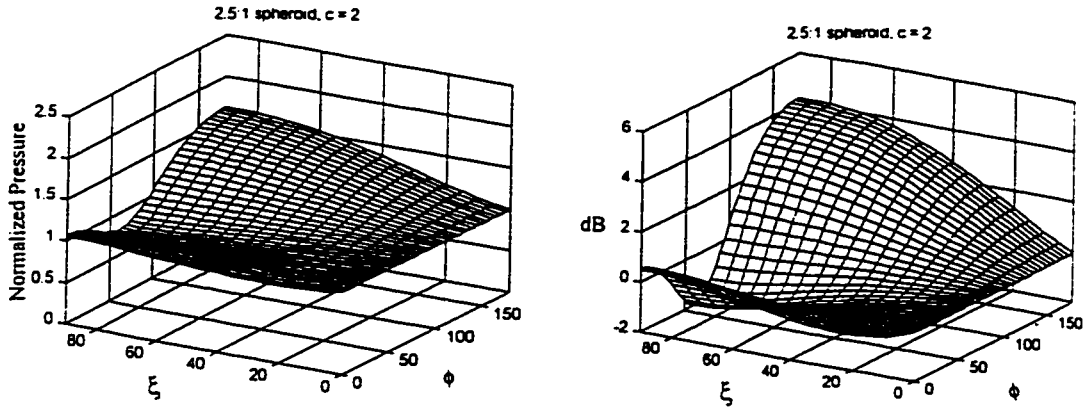
Figure 5.18 - Response of a 1060 Hz plane wave incident a prolate spheroidal head model. Raw amplitude is shown in the left plot, and decibels in the right. Elevation is plotted along the left edge, and azimuth along the right edge. The ear is located at 90 degrees elevation, and at 180 degrees azimuth (the back corner).
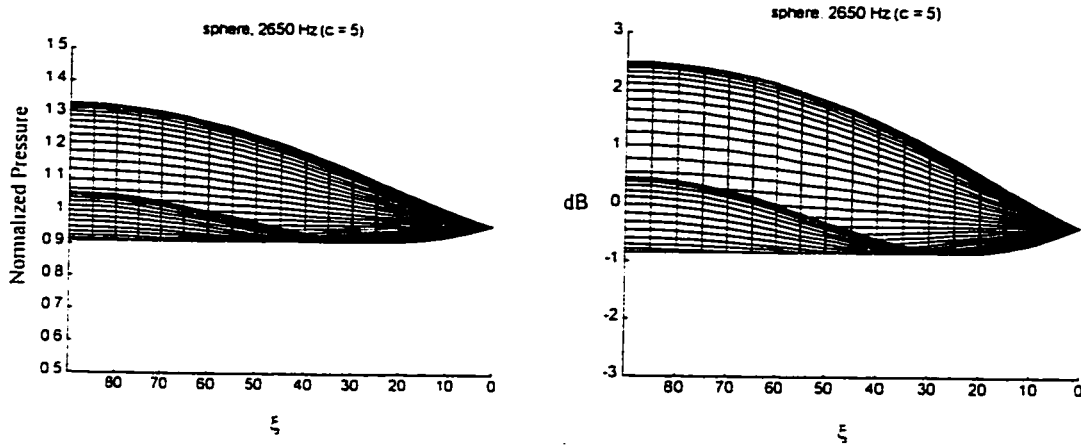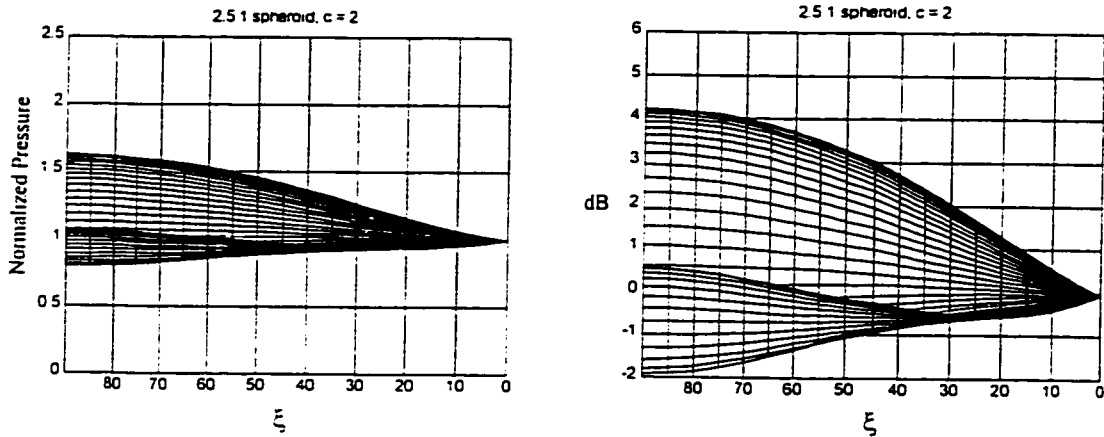

Figure 5.19 - Response of a 1060 Hz plane wave incident a prolate spheroidal head model. These plots are the same as those appearing in figure 5.18 except only the elevation effects are seen.
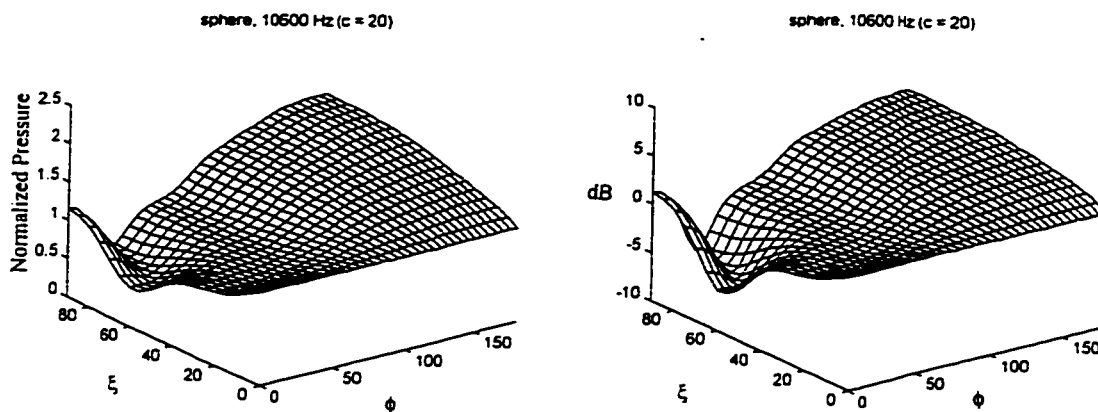
2.5:1 spheroid. c = 3

2.5 1 spheroid. c = 3
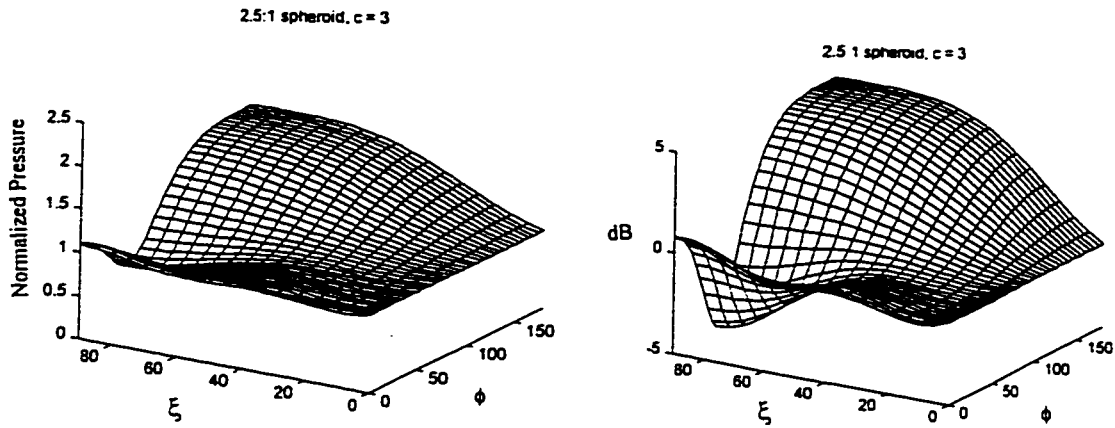
Figure 5.20 - Response of a 1590 Hz plane wave incident a prolate spheroidal head model. Raw amplitude is shown in the left plot, and decibels in the right. Elevation is plotted along the left edge, and azimuth along the right edge. The ear is located at 90 degrees elevation, and at 180 degrees azimuth (the back corner).

2.5 1 spheroid. c = 3

2.5:1 spheroid. c = 3
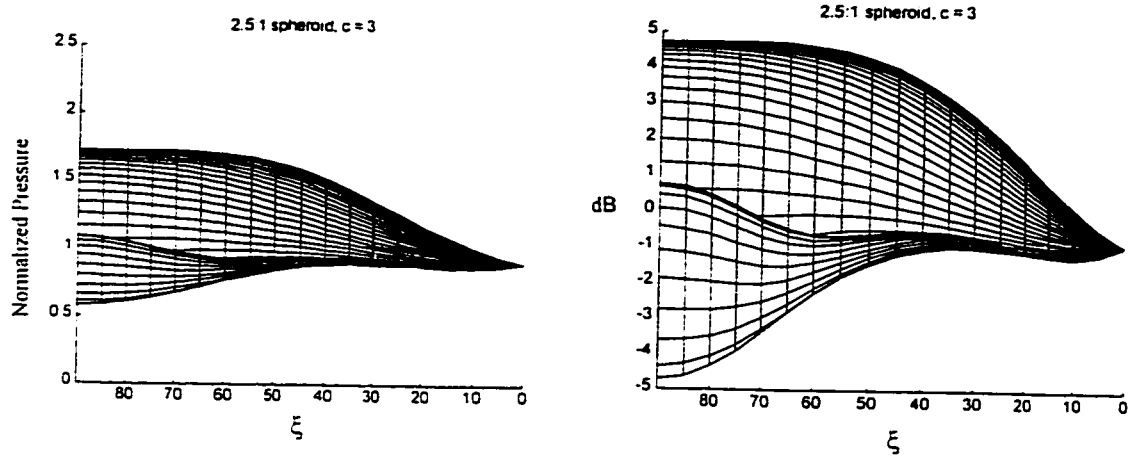
Figure 5.21 - Response of a 1590 Hz plane wave incident a prolate spheroidal head model. These plots are the same as those appearing in figure 5.20 except only the elevation effects are seen.
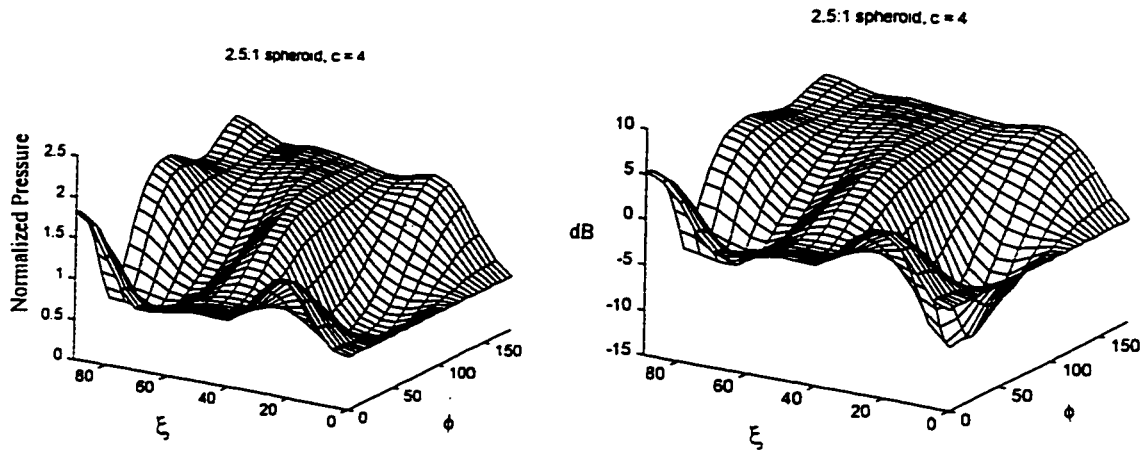
Figure 5.22 - Response of a 2120 Hz plane wave incident a prolate spheroidal head model. Raw amplitude is shown in the left plot, and decibels in the right. Elevation is plotted along the left edge, and azimuth along the right edge. The ear is located at 90 degrees elevation, and at 180 degrees azimuth (the back corner).
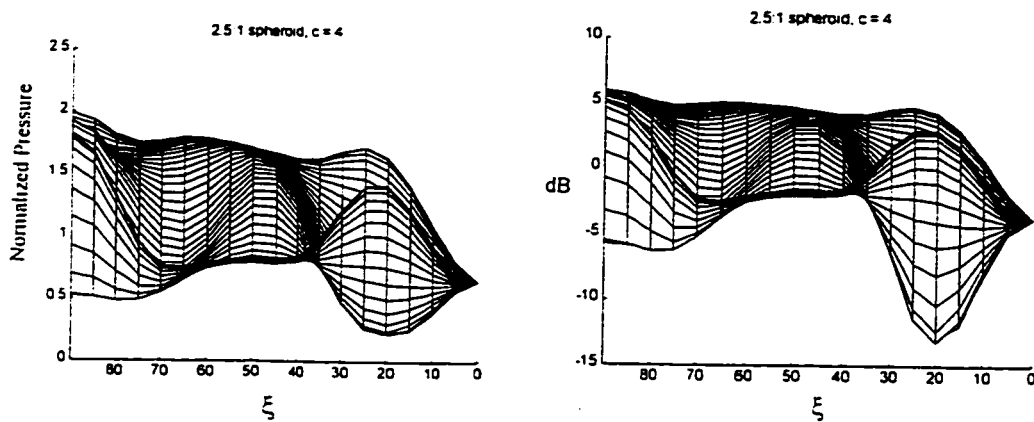
Figure 5.23 - Response of a 2120 Hz plane wave incident a prolate spheroidal head model. These plots are the same as those appearing in figure 5.22 except only the elevation effects are seen.
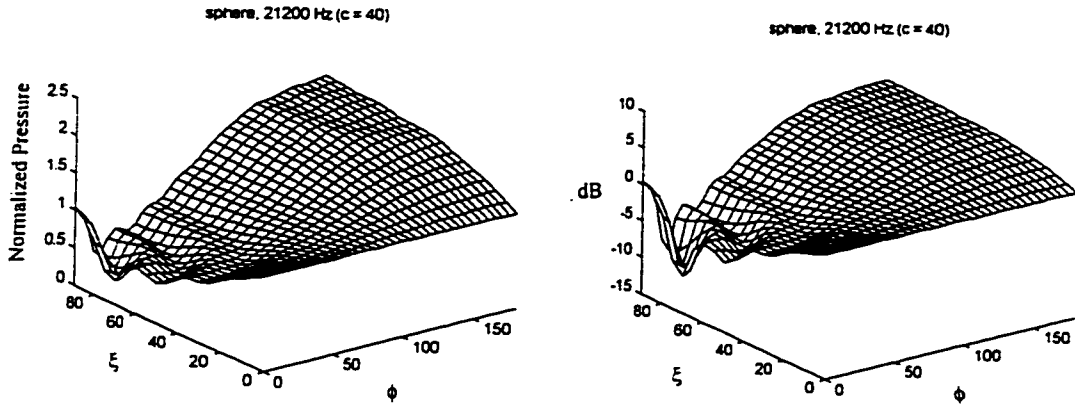
2.5:1 spheroid, c = 5

2.5:1 spheroid, c = 5
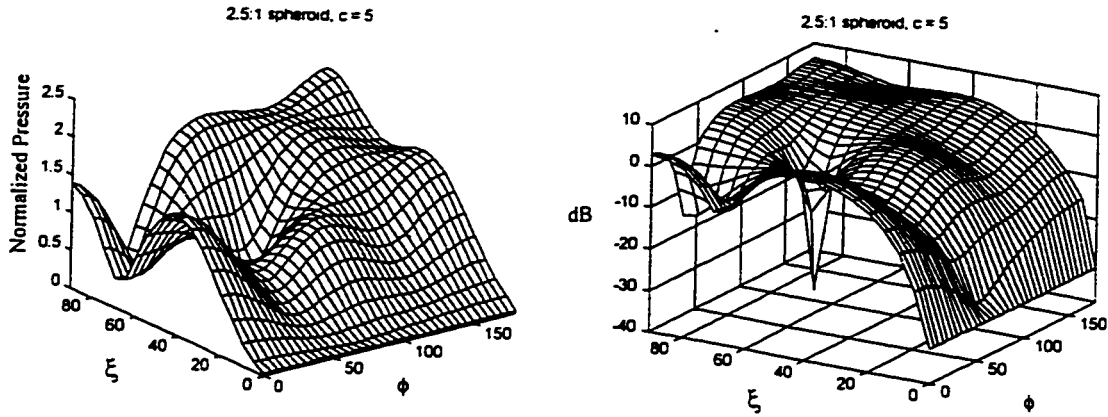
Figure 5.24 - Response of a 2650 Hz plane wave incident a prolate spheroidal head model. Raw amplitude is shown in the left plot, and decibels in the right. Elevation is plotted along the left edge, and azimuth along the right edge. The ear is located at 90 degrees elevation, and at 180 degrees azimuth (the back corner).
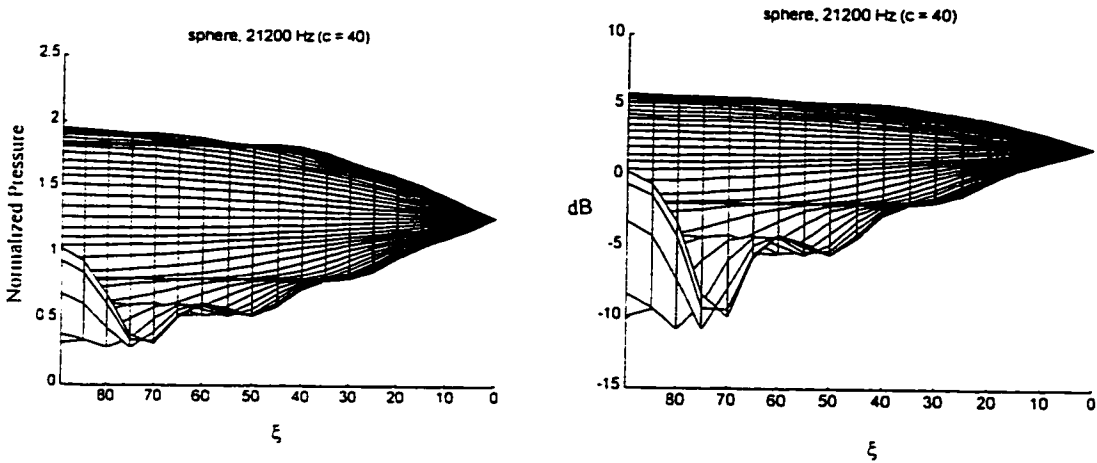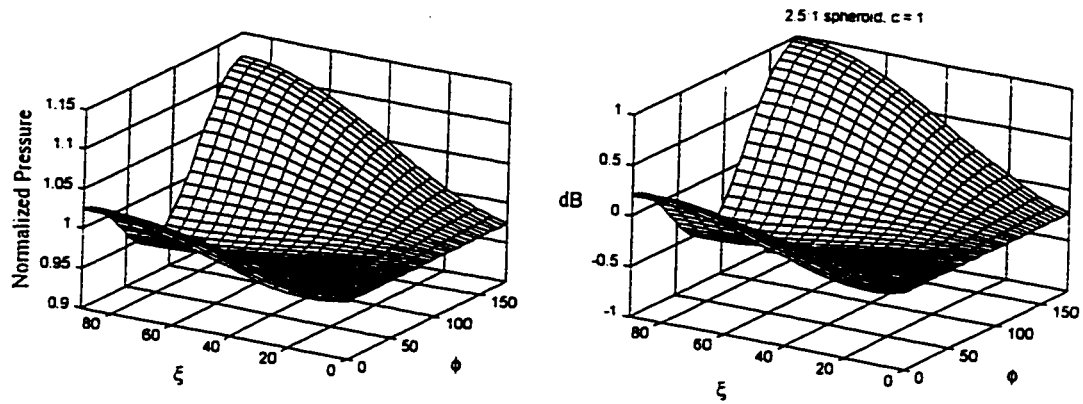
2.5 1 spheroid, c = 5

2.5 1 spheroid, c = 5
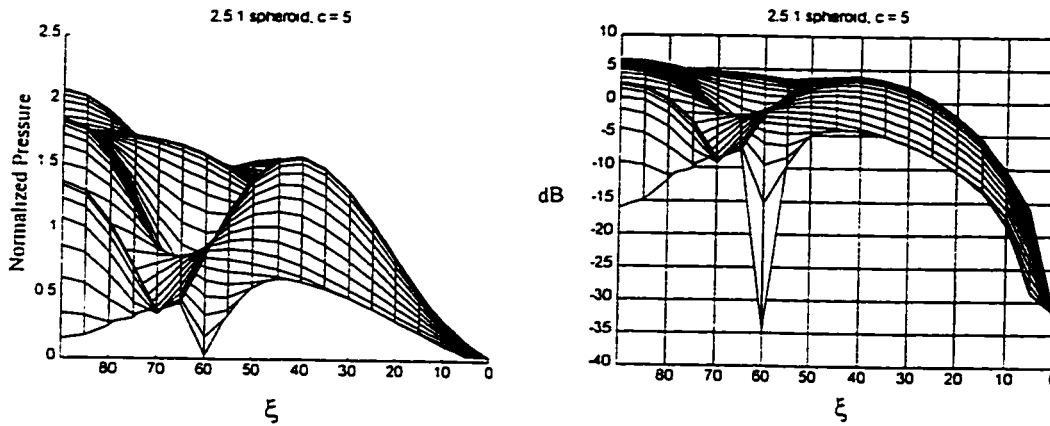
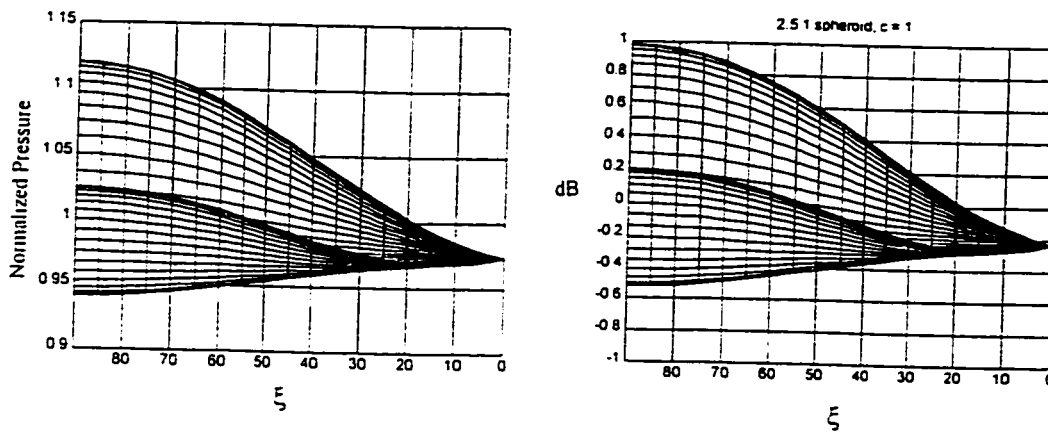**Figure 5.25 - Response of a 2650 Hz plane wave incident a prolate spheroidal head model. These plots are the same as those appearing in figure 5.24 except only the elevation effects are seen.**

It is of great interest that the spherical model was never subjected to frequencies high enough to cause a 6 dB gain at the point of incidence. The spheroid, on the other hand, did achieve the 6 dB increase with relatively low frequencies.

One possible explanation is that there is an error in one of the MATLAB® routines. The algorithms were thoroughly checked several times, and this has been dismissed as being the cause. Still, this possibility warrants some comment. The most likely error is that of head dimension being off by a factor of 2 (i.e., using a diameter instead of a radius). This was examined by testing different head sizes with the spherical model. Head size being fixed for the spheroidal model forced changing it in the spherical model. None of these sizes produced results anything like the spheroidal model. Also, the fact that the sphere still hasn't achieved the 6 decibel gain by $c = 40$ would indicate that head size is not the issue, since it has already been pointed out that increasing frequency and radius are mathematically the same action .

The response of the spheroidal model as a function of continuous frequency is not known. There could be some overlooked physics involved which drastically changes the shape of the response with frequency as the eccentricity of the spheroid increases. One possibility is that the spheroid causes scattering to be mostly restricted to the azimuthal directions. The sphere scatters with circular symmetry by virtue of its shape. Perhaps more energy is lost to space in the spherical case. Moving toward a rounder, more head-like shape, should alter the response surface of the spheroidal model closer to that of the spherical model. The limited head-shape options drastically hamper understanding of why the spheroidal model achieves the 6 decibel gain at such a low frequency. It should to be thoroughly investigated with an algorithm that allows something similar to figure (1.2) to be created.

The other, and probably more important difference in the responses of the two models, is the 35 dB trough on the spheroid plot for $c = 5$. Along with the interesting ripples that begin appearing around $c = 3$, this trough is clearly important to the response of the spheriodal HRTF at this frequency. There is a dip in the $c = 4$ plot that occurs at an elevation far closer to the top of the head (for waves incident at roughly the temple). Is this the same feature as the spike when $c = 5$? With the ability to expand the coefficients d_r^{mn}, as described in chapter 3, it should be possible to investigate if, where, and under what conditions this trough moves. If this is indeed the same feature, it could be fundamental to how humans localize sound in elevation, particularly sounds that are not monochromatic.

6.2 Conclusion

In order to provide a more useful tool for comparison of the response to the spherical and prolate spheriodal HRTF models, the decibel response surfaces have been reproduced to the same scale and placed side-by-side.

sphere. 530 Hz (c = 1)
2.5:1 spheroid, c = 1
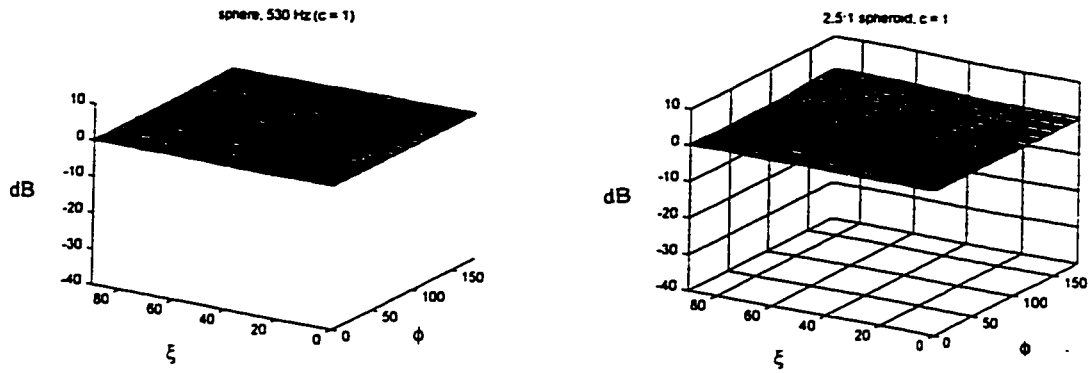
Figure 5.26 - Side-by-side comparison of response of the sphere (left) and spheroid (right) model HRTF to an incoming plane wave of 530 Hz. Both responses are quite flat and strikingly similar for this low frequency.

sphere. 1060 Hz (c = 2)
2.5:1 spheroid, c = 2
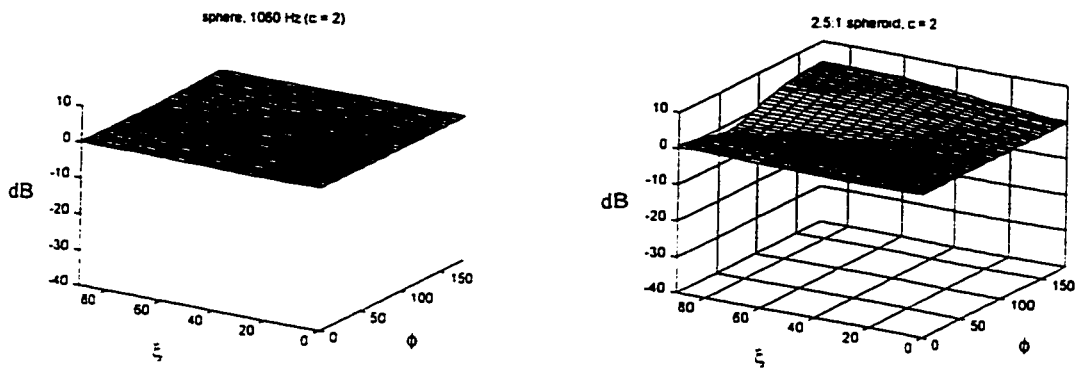
Figure 5.27 - Side-by-side comparison of response of the sphere (left) and spheroid (right) model HRTF to an incoming plane wave of 1060 Hz. Both responses are still quite flat, but the response to the spheroid is beginning to exhibit the first signs of high-frequency behavior.

sphere, 1590 Hz (c = 3)

2.5.1 spheroid, c = 3
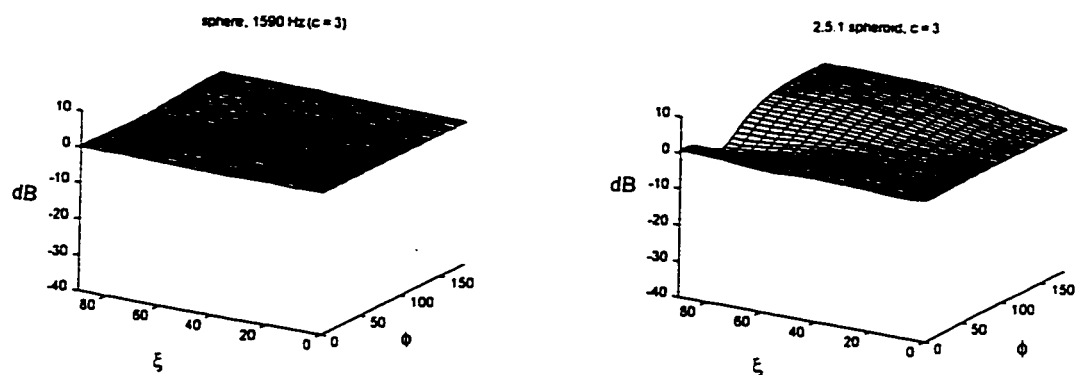
Figure 5.28 - Side-by-side comparison of response of the sphere (left) and spheroid (right) model HRTF to an incoming plane wave of 1590 Hz. The response to the spherical model is still quite flat, but the spheroidal model is really starting to show high-frequency effects, including a narrowing of the so-called "bright spot" at the left-most part of the plot.

sphere, 2120 Hz (c = 4)

2.5 1 spheroid, c = 4
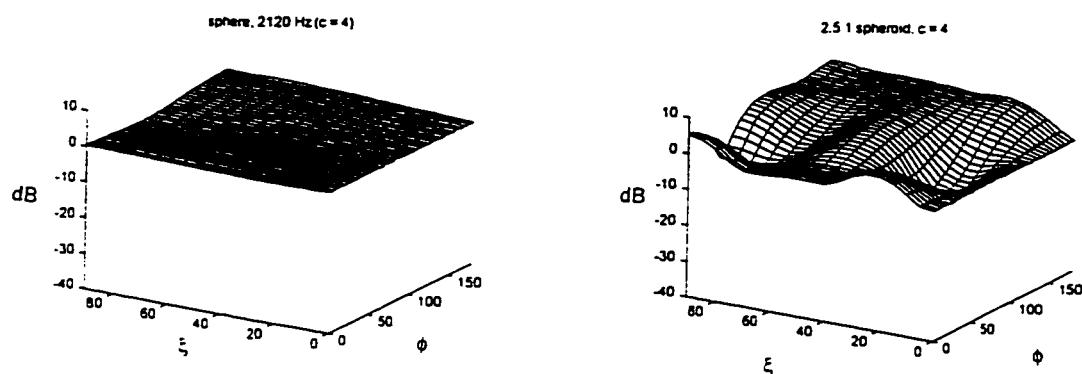
Figure 5.29 - Side-by-side comparison of response of the sphere (left) and spheroid (right) model HRTF to an incoming plane wave of 2120 Hz. The response to the spherical model is flat even at this frequency, though it is apparent that the so-called "bright-spot" is beginning to narrow. Although it has been narrowing with each increment in frequency, this is the first time that the effect is quite noticeable. This is the first indication of higher-frequency behavior in the spherical model, but the spheroidal model already exhibits interesting ripples.

sphere, 2650 Hz (c = 5)

2.5:1 spheroid, c = 5
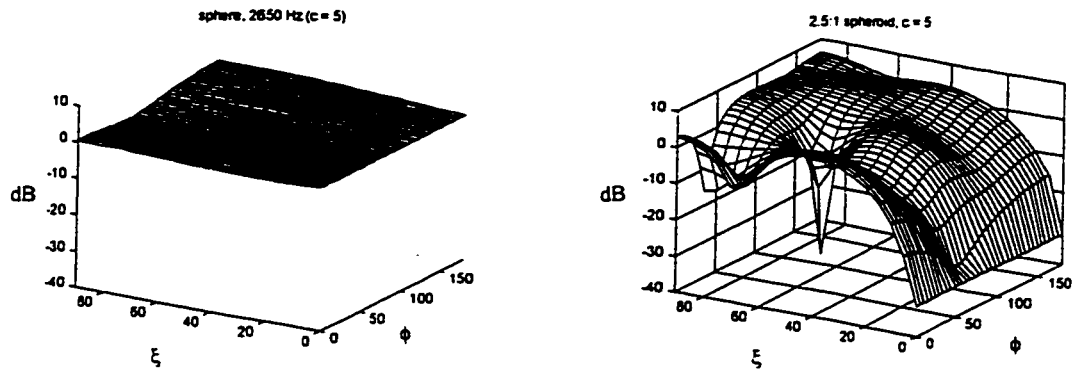
Figure 5.30 - Side-by-side comparison of response of the sphere (left) and spheroid (right) model HRTF to an incoming plane wave of 2650 Hz. The response to the spherical model is beginning to move noticeably away from flatness, and the so-called "bright-spot" continues to narrow. By this point, the spheroidal model exhibits some extraordinary behavior.

sphere, 21200 Hz (c = 40)

2.5 1 spheroid, c = 5
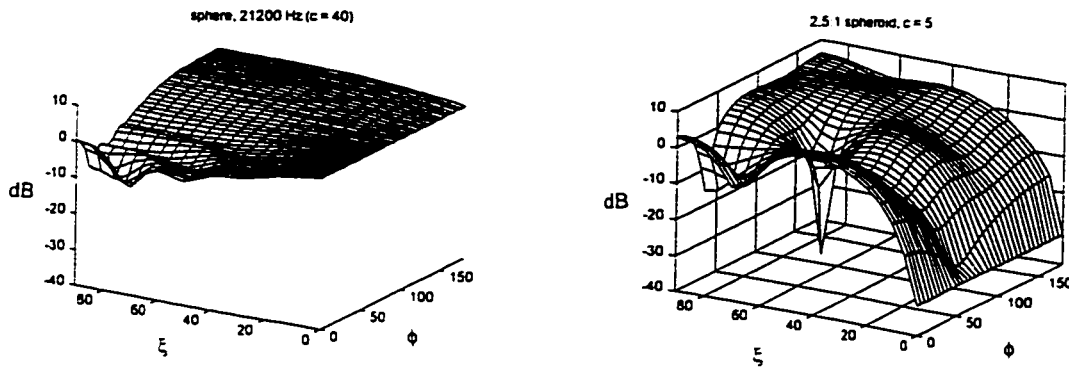
Figure 5.31 - Side-by-side comparison of response of the spherical HRTF model to an incoming plane wave of 21200 Hz, (left) and of the response to the spheroid HRTF model to an incoming plane wave of 2650 Hz (right). Even with the frequency of the incoming wave almost an order of magnitude higher, the spherical model produces only some ripples with circular symmetry.

Clearly, the work incorporated into this thesis is a mere fraction of what is necessary for incorporation of the prolate spheroidal head into a working HRTF model that can synthesize binaural sound. A great deal of work needs to be completed before that can become a reality. A list of several items that need attention appears below.

- Conversion of the look-up tables to series expansions of the coefficients d_r^{mn} is needed in order to allow any value of ξ to be used in a computer algorithm. It would require a great deal of work to expand these coefficients by hand to allow them to be placed into a generic look-up table routine, that would pass in the value of c to produce the required coefficient d_r^{mn}.

- Duplication of the work published by Duda and Martens using the prolate spheroid at several elevations is necessary to characterize how the spheroid affects the shape of the frequency response. Results from this thesis indicates the 6 decibel gain occurs at far lower frequencies with the spheroid than with the sphere. This attribute needs to be verified and understood. The cause for such an unexpected response is not intuitively obvious.

- Investigation of the effects of range is critical to the HRTF model. With a look-up table as described in the first bullet, a point source can be used instead of a plane wave. Bowman, Senior, and Uslenghi provide the necessary algorithms to proceed if the required values of ξ can be solved. That look-up table would allow this type of generic spheroid to be considered.

- Physical construction of a spheroid head model, and measurement the real response from it, is an important step toward verification of the mathematical model.

- Study of a spheroid as close as possible to the shape of the human head is another obvious step. These results should be compared to those from the spherical model, and those presented in this thesis. It is reasonable to expect that as ξ_1 approaches infinity—the spheroid becoming a sphere—the response of the HRTF will more and more closely resemble that of the spherical model.

- Incorporation of pinna models and other effects into the spheroidal HRTF model, and generation of binaural sound from this compound model, should be the culmination of all the aforementioned work.

- Finally, the differences between using a prolate spheroid and a triaxial ellipsoid must be investigated. A third dimension of asymmetry will affect both elevation and azimuthal effects. The HRTF must ultimately model the human head more and more closely, and the triaxial ellipsoid is one step closer than the prolate spheroid. A discussion of preliminary work with the triaxial ellipsoid, which was done in conjunction with this thesis, is presented in Appendix A.

The results presented above demonstrate that modeling the human head with a prolate spheroid adds some response characteristics fundamentally different from those of the sphere. The prolate spheroid model, representing an elongated head, produces interesting constructive and destructive interference patterns in frequency response at far lower frequencies than does the spherical model. The 6 dB gain at the point of incidence appears to be achieved at lower frequencies as well, and the reasons for this are not

intuitively obvious. There is a deep trough at the highest frequency investigated, which possibly moves to different locations of the response surface with frequency. The response of the prolate spheroidal HRTF model is sufficiently different from that of the spherical model to warrant further study.

Bibliography

Milton Abramowitz, Irene A. Stegun, Handbook of Mathematical Functions. National Bureau of Standards: 1964; reprint, New York: Dover, 1972.

J. J. Bowman, T. B. A. Senior, P. L. E. Uslenghi, eds. Electromagnetic and Acoustic Scattering by Simple Shapes. 2d ed. New York: Summa, 1987.

   This book is a gold mine of information on acoustic scattering for all simple shapes except the triaxial ellipsoid.

C. P. Brown, "Modeling the Elevation Characteristics of the Head-Related Impulse Response," M.S. Thesis, Dept. of Elec. Engr., San Jose State Univ., May 1996.

Richard O. Duda, William L. Martens, "Range Dependence of the HRTF for a Spherical Head." Proc. 1997 IEEE Workshop on Applications of Signal Processing to Audio and Acoustics. (Mohonk, NY October 1997).

_____, "Range Dependence of the Response of a Spherical Head Model." Submitted for publication in the J. Acoust. Soc. Amer.

Carson Flammer, Spheroidal Wave Functions. Stanford: Stanford University Press, 1957.

   This book defines the functions and notation used throughout this thesis, as well as in most of the references which present information pertaining to same.

H. E. Hunter, D. B. Kirk, T. B. A. Senior, E. R. Wittenberg, Tables of Prolate Spheroidal Functions for m = 0: Volume I. Ann Arbor: University of Michigan Radiation Laboratory Report No. 7133-1-T (AD-619979).

_____, Tables of Prolate Spheroidal Functions for m = 0: Volume II. Ann Arbor: University of Michigan Radiation Laboratory Report No. 7133-1-T (AD-619979).

   These two volumes contain extensive tabulations for $m = 0$, along with source code for their generation, and a brief description of the mathematics supporting it. Tabulations for a rounder spheroid than that used in this thesis is available in this report, which was received too late for incorporation into this work. The author's copy has been given to the SJSU EE Department.

Jon Mathews and R. L. Walker, Mathematical Methods of Physics. 2d ed. Redwood City: Addison-Wesley, 1970.

Contains a worked example of expanding a continued fraction into a Taylor series as it applies to Mathieu functions.

Mathworks, Inc., The, <u>Student Version of MATLAB® Version 4 User's Guide</u>. Englewood Cliffs, N.J.: Prentice-Hall, 1995.

Philip M. Morse, Herman Feshbach, <u>Methods of Theoretical Physics</u>. New York: McGraw-Hill, 1953.

Contains a wealth of information on both the prolate spheroid and triaxial ellipsoid, and all relevant functions, however, their notation is different from that of Flammer, and the book much more rigorous.

T. B. A. Senior, "Scalar Diffraction by a Prolate Spheroid at Low Frequencies." <u>Can. J. Phys.</u> 38 (1960): 1632-41.

This paper presents series expansions of several d_r^{mn} coefficients.

T. B. A. Senior, to Richard W. Novy, fax transmission of calculations for series expansion of d_0^{00}, (28 January 1998): In hands of both Novy and Senior.

Murray R. Spiegel, <u>Mathematical Handbook of Formulas and Tables</u>. Schaum's Outline Series in Mathematics. New York: McGraw-Hill, 1968.

K. Sugiyama, "Diffraction Coefficients of Prolate Spheroids." <u>J. Acoust. Soc. Jpn.</u> 45 No. 7 (July 1989): 527-33.

This paper is in Japanese.

A. N. Tikhonov and A. A. Samarskii. <u>Equations of Mathematical Physics.</u> Oxford: Pergamon Press, 1963; reprint, New York: Dover, 1990.

Contains a nice worked example of acoustic plane wave diffraction by a sphere.

Appendix I - HRTF Using a Triaxial Ellipsoid

The obvious next extension to the HRTF model, beyond using a prolate spheroid for head shape, is to use a triaxial ellipsoid. This introduces several difficulties that aren't encountered with any of the models previously discussed. Since this thesis project began with the intention of bypassing the prolate spheroid and going directly to the triaxial ellipsoid, quite a bit of information was gained that warrants discussion. It is hoped that this appendix will assist a future researcher locate appropriate references, and provide some insight into the approach used. The triaxial ellipsoid model was abandoned only because it became clear that insufficient time was available to complete it.

The two main approaches to this problem are to use differential equations or integral equations to solve it. From literature and Internet searches, it quickly became apparent that the integral equation approach is by far the most common. Although the work is, for the most part, understandable, the methods used are relatively advanced integral equation techniques. Since the work done in spherical coordinates (and now prolate spheroidal coordinates) all uses differential equation methods, it made sense to search for information on a differential approach to the problem.

Before mentioning the numerical solution that was finally discovered, it is appropriate to first summarize the coordinate system and its idiosyncrasies. The triaxial ellipsoidal coordinate system is the most general of all the eleven orthogonal coordinate systems. The other ten are degenerate forms of it [Morse and Feshbach 1953]. The

triaxial ellipsoid is the only coordinate surface of all these coordinate systems that cannot be formed as a surface of revolution, and as such, is the most complicated simple surface for which diffraction problems of this sort can be solved by separation of variables.

The coordinate system itself is formed by a set of confocal and orthogonal triaxial ellipsoids, hyperboloids of one sheet, and hyperboloids of two sheets. A point is specified by identifying one of each, but this is only sufficient to identify the point within any particular octant of the Cartesian coordinate system. This is because there are eight points at which these all intersect. This problem was overcome by enforcing boundary conditions at the Cartesian planes on the Lamé wave functions, which are the triaxial ellipsoid equivalent of the radial and angular prolate spheroidal wave functions.

Specifics on the Lamé wave functions, the aforementioned boundary conditions, and the Helmholz equation in ellipsoidal coordinates are out of the scope of this thesis. They are well documented in the references listed at the end of this appendix, and are quite easy to understand in the context of the computational methods used.

The main difficulty in working with the Lamé wave differential equations is the identification of their eigenvalues. Without this information, the proper Lamé wave function solutions cannot be identified. The eigenvalues are found with the help of an auxiliary system of ordinary differential equations, which must be solved computationally. For the work done prior to abandoning this head shape, Runge-Kutta routines were employed. The solution to this system of ordinary differential equations is an estimate of the eigenvalue for the Lamé wave equation. This estimate is fed into what

is referred to as a "two-dimensional fork method" for finding the proper eigenvalue [Abramov, et. al. 1989]. This is a self-correcting algorithm which slices off regions of the plane until the correct answer is known within a predetermined tolerance.

The boundary conditions at the Cartesian planes introduce a nine-term representation of the solution to the Helmholz equation at any given point, but in many cases several of those terms are zero. Further explanation of the process of generating a solution to the problem of a plane wave scattering from the triaxial ellipsoid—from which the HRTF model is constructed—is again left to the references below. They are quite well written, and relatively easy to follow. The caveat to that statement is that these papers were originally written in Russian, and the references below point to the English translations. The first three references are essential to anyone pursuing this type of research, and the other references are of supplemental interest. It should be noted that the journal most of these papers were published in changed names from *U.S.S.R. Computational Mathematics and Mathematical Physics*, to simply, *Computational Mathematics and Mathematical Physics*, at about the same time as the breakup of the Soviet Union.

Bibliography of Works Involving Triaxial Ellipsoids

Essential Works

A. A. Abramov, A. L. Dyshko, N. B. Konyukhova, T. V. Levitina, "A Numerical-Analytic Investigation of the Diffraction of a Plane Acoustic Wave by Ideal Prolate Spheroids and Triaxial Ellipsoids," Comp. Maths Math. Phys. 35 No. 9 (September 1996): 1103-1123.

_____, "Computation or Radial Wave Functions for Spheroids and Triaxial Ellipsoids by the Modified Phase Function Method," Comp. Maths Math. Phys. 31 No. 2 (February 1992): 25-42.

_____, "Evaluation of Lame Angular Wave Functions by Solving Auxiliary Differential Equations," U.S.S.R. Comp. Maths Math. Phys. 29 No. 3 (March 1989): 119-131.

Supplemental Works

Aleksander A. Abramov, Nadezhda B. Konyukhova, Tatyana V. Levitina, "Numerical Investigation of the Problem of a Plane Acoustic Wave Scattering by a Triaxial Ellipsoid," Proc. 1995 ASME Design Engineering Technical Conferences. 3 Part B New York: (1995).

George Dassios, "Convergent Low Frequency Expansions for Penetrable Scatterers," J. Math. Phys. 18 No. 1 (January 1991): 126-37.

A rigorous treatment of the triaxial ellipsoid problem using integral equations.

T. V. Levitina, "The Conditions of Applicability of an Algorithm for Solving Two-Parameter Self-Adjoint Boundary Value Problems," Comp. Maths Math. Phys. 31 No. 5 (May 1991): 34-40.

T. Levitina, E. J. Brandas, "Partial Waves in the Nonspherical Case," International Journal of Quantum Chemistry: Quantum Chemistry Symposium, 30 (1996): 5-9.

Appendix B - MATLAB® Code

HRTFSPH.M

```
% This is a script file to calculate the HRTF of a sphere.
%
%
% Syntex is HRTFSPH
%
%
% Produced in process of completion of masters thesis,
% Department of General Engineering, San Jose State University
% MATLAB function (c) Richard W. Novy, 1997-8
%

clear;
clg;
holdtime = cputime;
c0 = 343; % m/s
omega = 21200;  %Hz, equivilent to c = 1
k = omega/c0;;
a = .111  % radius of sphere size of prolate
        % spheriod in the large dimension,
        % worst case for high frequency effects.
ka = k*a;

phi = zeros(1,37);
zeta = zeros(1,37);
zeta2 = zeros(1,19);
rrr = 0:36;
nnn = 1:19;
phi = (rrr*pi/36);
zeta = (rrr*pi/36);
zeta2(nnn) = zeta(nnn);
ViVs = zeros(19,37);


for ss = 1:19
ss
 for tt = 1:37
 tt
```

```
  theta = acos(cos(phi(tt))*cos(pi/2-zeta(ss)));
  scale_factor = i/(ka^2);
  sum = 0;
  for n = 0:10
    constant = (2*n+1)*(-i)^n;
    P = legendre(n,cos(theta));
    PP = P(1);
    hprime = (n/ka)*(spherej(n,ka)+i*spherey(n,ka)) -
(spherej(n+1,ka)+i*spherey(n+1,ka));
    sum = sum + constant*PP/hprime;
  end


  ViVs(ss,tt) = abs(scale_factor*sum);
  end

%plot(phi,ViVs(ss,:))
%hold on
%drawnow

end
ViVs = fliplr(ViVs);
% ViVs = 20*log10(ViVs);   %convert to dB

phi = phi * 180/pi; % convert to degrees
zeta2 = zeta2 * 180/pi; % convert to degrees

mesh(phi,zeta2,ViVs)
shading interp
colormap(cool);
% axis([0 180 0 90 -40 10]);  % For dB response
 axis([0 180 0 90 0 2.5]);  % Natural amplitude response
title('sphere, 21200 Hz (c = 40)');

total_time = cputime - holdtime
```

SPHEREJ.M

```
function [j] = spherej(alpha,x)
%
% The function spherej calculates the spherical bessel function
% of the first kind, order alpha, with argument x.
%
% syntex:
%       [j] = spherej(alpha,x)
%
%
%
%
% Produced in process of completion of masters thesis,
% Department of General Engineering, San Jose State University
% MATLAB function (c) Richard W. Novy, 1997
%
%
% Constrcted from the algorithms in "Handbook of Mathematical Functions"
%   by Abramowitz and Stegun, Dover, 1962
%


[j] = sqrt(pi/2/x)*besselj(alpha+0.5,x);
```

SPHEREY.M

```
function [y] = spherey(alpha,x)
%
% The function spherey calculates the spherical bessel function
% of the second kind, order alpha, with argument x.
%
% syntex:
%       [y] = spherey(alpha,x)
% where:
%       alpha = order of spherical bessel function
%       x = argument
%
% Produced in process of completion of masters thesis,
% Department of General Engineering, San Jose State University
% MATLAB function (c) Richard W. Novy, 1997
%
% Constrcted from the algorithms in "Handbook of Mathematical Functions"
%   by Abramowitz and Stegun, Dover, 1962
%

[y] = sqrt(pi/2/x)*bessely(alpha+0.5,x);
```

HRTFDUDA.M

```
% This is a script file to duplicate Duda's results.
%
% syntex:  HRTFDUDA
%
% Produced in process of completion of masters thesis,
% Department of General Engineering, San Jose State University
% MATLAB function (c) Richard W. Novy, 1997
%

clear;
clg;
holdtime = cputime;
c0 = 343; % m/s
a = .54  %To match Duda's plot
% ka = k*a;

phi = zeros(1,37);
zeta = zeros(1,37);
zeta2 = zeros(1,19);
rrr = 0:36;
nnn = 1:19;
phi = (rrr*pi/36);
zeta = (rrr*pi/36);
zeta2(nnn) = zeta(nnn);
ViVs = zeros(37,28);
ss = 19;

for tt = 1:37
tt

 for freqcnt = 1:28

  if freqcnt < 11
    omega = 100 * freqcnt;   % 100 - 1000 Hz range
    k = omega/c0;
    ka = k*a;
  elseif freqcnt < 20
    omega = 1000 * (freqcnt - 9); % 2000 - 10000 Hz range
    k = omega/c0;
```

```
    ka = k*a;
  elseif freqcnt < 29
    omega = 10000 * (freqcnt - 18);   % 20000 - 100000 Hz range
    k = omega/c0;
    ka = k*a;
  end
  omega
  tt
  ka

  theta = acos(cos(phi(tt))*cos(pi/2-zeta(ss)));
  scale_factor = i/(ka^2);
  sum = 0;

  if ka < 1
    for n = 0:10
      constant = (2*n+1)*(-i)^n;
      P = legendre(n,cos(theta));
      PP = P(1);
      hprime = (n/ka)*(spherej(n,ka)+i*spherey(n,ka)) -
                  (spherej(n+1,ka)+i*spherey(n+1,ka));
      sum = sum + constant*PP/hprime;
    end
  elseif ka < 5
    for n = 0:30
      constant = (2*n+1)*(-i)^n;
      P = legendre(n,cos(theta));
      PP = P(1);
      hprime = (n/ka)*(spherej(n,ka)+i*spherey(n,ka)) -
                  (spherej(n+1,ka)+i*spherey(n+1,ka));
      sum = sum + constant*PP/hprime;
    end
  elseif ka < 10
    for n = 0:70
      constant = (2*n+1)*(-i)^n;
      P = legendre(n,cos(theta));
      PP = P(1);
      hprime = (n/ka)*(spherej(n,ka)+i*spherey(n,ka)) -
                  (spherej(n+1,ka)+i*spherey(n+1,ka));
      sum = sum + constant*PP/hprime;
    end
  elseif ka < 25
    for n = 0:150
```

```
        constant = (2*n+1)*(-i)^n;
        P = legendre(n,cos(theta));
        PP = P(1);
        hprime = (n/ka)*(spherej(n,ka)+i*spherey(n,ka)) -
                 (spherej(n+1,ka)+i*spherey(n+1,ka));
        sum = sum + constant*PP/hprime;
      end
    elseif ka < 40
      for n = 0:200
        constant = (2*n+1)*(-i)^n;
        P = legendre(n,cos(theta));
        PP = P(1);
        hprime = (n/ka)*(spherej(n,ka)+i*spherey(n,ka)) -
                 (spherej(n+1,ka)+i*spherey(n+1,ka));
        sum = sum + constant*PP/hprime;
      end
    elseif ka > 39
      for n = 0:250
        constant = (2*n+1)*(-i)^n;
        P = legendre(n,cos(theta));
        PP = P(1);
        hprime = (n/ka)*(spherej(n,ka)+i*spherey(n,ka)) -
                 (spherej(n+1,ka)+i*spherey(n+1,ka));
        sum = sum + constant*PP/hprime;
      end
    end


    plotomega(freqcnt) = omega;
    ViVs(tt,freqcnt) = 20*log10(abs(scale_factor*sum));
  end %end freqcnt loop

% Trying to normalize like duda

plotomega = plotomega*a/c0;

  semilogx(plotomega,ViVs(tt,:),'g')
  title('Frequency Response by Angle, 8.75 cm sphere')
  xlabel('Frequency'), ylabel('Response in dB')
  hold on
  drawnow

end %end tt loop
```

```
% ViVs = fliplr(ViVs);
% ViVs = 20*log10(ViVs);   %convert to dB
% ViVs = 20*log10(ViVs);

% mesh(phi,zeta2,ViVs)
% shading interp
% colormap(cool);
% title('sphere, 130000 Hz');
% total_time = cputime - holdtime
% end
% end
```

HRTF.M

```
%
% This is a script file to calculate the head-related transfer function (HRTF)
% of a prolate spheroidal model head. The equation for Vi + Vs on the
% surface of the spheroid is given   in "Electromagnetic and Acoustic
% Scattering by Simple Shapes" by J.J. Bowman, T.B.A. Senior, and P.L.E. Uslenghi
% Hemisphere Publishing Corporation, 1987
%
% Produced in process of completion of masters thesis,
% Department of General Engineering, San Jose State University
% (c) Richard W. Novy, 1997
%
clear;
holdtime = cputime;
% Head shape is 22.2 cm by 8.25 cm
clg;
sound_speed = 343; % m/s
omega = 530;  %Hertz

c = 1; %  This was a living document, change c as needed.

xi1 = 1.077;  % Forced upon us by virtue of being roundest value available.
% zeta = pi/2;  % Incident angle measured down from z-axis
eta = 0; % Altitude coordinate of ear (selects hyperboloid of choice)
%phi = pi; % Azimuthal coordinate of ear.  (When sound moves, phi actually moves).

scale_factor = 2/(c*(xi1^2-1)); % Part of the equation outside the sum.
phi = zeros(1,37);
zeta = zeros(1,37);
zeta2 = zeros(1,19);
rrr = 0:36;
nnn = 1:19;
phi = (rrr*pi/36);
zeta = (rrr*pi/36);
zeta2(nnn) = zeta(nnn);
ViVs = zeros(19,37);
for ss = 1:19
for tt = 1:37
ss
tt
%for ss = 1:19
```

```
%ss
sum = 0;
for m = 0:3
  for n = m:3
   % fprintf('.');
    ep = epsilon(m);
    norm = i^(n+1)/N(m,n,c);
    r3prime = lookuprp(m,n,c);
    S_zeta = s_angle(m,n,c,cos(zeta(ss)));
    S_eta = s_angle(m,n,c,eta);
    azimuth = cos(m*phi(tt));
    sum = sum + ep*norm*S_zeta*S_eta*azimuth/r3prime;
  end
end
ViVs(ss,tt) = abs(sum * scale_factor);
% ViVs
end
%plot(phi,ViVs(ss,:))
%hold on
%drawnow
end
phi = phi*180/pi;
zeta2 = zeta2*180/pi;

%xlabel('elevation (radians)');
%ylabel('normalized pressure at ear');
ViVs = 20*log10(ViVs);
mesh(phi,zeta2,ViVs)
shading interp
colormap(cool);
title('2.5:1 spheroid, c = 1');
total_time = cputime - holdtime
```

EPSILON.M

```
%
function [ep] = epsilon(m)
%
% The function epsilon is the Neumann symbol.
% It returns 1 if m = 0, otherwise returns 2.
%
% Syntex:
%      ep = epsilon(m)
%
% Where:
%      m = degree of spheroidal wave function
%
% Function taken from the book Electromagnetic and Acoustic Scattering
% by Simple Shapes, by J.J. bownam, T.B.A. Senior, and P.L.E. Uslenghi,
% Hemisphere Publishing Corporation, 1969, Rev. 1987
%
% Produced in process of completion of masters thesis,
% Department of General Engineering, San Jose State University
% MATLAB function (c) Richard W. Novy, 1997

if m == 0
 ep=1;
else
 ep=2;
end
```

LOOKUPRP.M

```
function R3prime = lookuprp(m,n,c)
%
% This function performs a look-up table operation
% to find the derivative of the radial spheroidal
% wave function R(3).
%
% Syntex:
%         d = lookuprp(m,n,c)
%
% where:
%    m = degree of spheroidal wave function
%    n = order of spheroidal wave function
%    c = Independent variable c=1/2*k*d  Currently this routine
%        only has lookup-tables integers c=1 through 5.
%
% R(3) = R(1) + i*R(2)
%
% R(3)' = R(1)' + i*R(2)'
%
% Tables taken from the book Spheroidal Wave Functions, by
% Carson Flammer, Stanford University Press, 1957
%
% Produced in process of completion of masters thesis,
% Department of General Engineering, San Jose State University
% MATLAB function (c) Richard W. Novy, 1997
%
%
%
if c == 1

  fid=fopen('c1r1pr.tab','r');
  c1r1pr=fscanf(fid,'%f',[4,4])';
  R1p=c1r1pr(m+1,n+1);
  status = fclose(fid);

  fid=fopen('c1r2pr.tab','r');
  c1r2pr=fscanf(fid,'%f',[4,4])';
  R2p=c1r2pr(m+1,n+1);
  status = fclose(fid);

elseif c == 2
```

```
fid=fopen('c2r1pr.tab','r');
c2r1pr=fscanf(fid,'%f',[4,4])';
R1p=c2r1pr(m+1,n+1);
status = fclose(fid);

fid=fopen('c2r2pr.tab','r');
c2r2pr=fscanf(fid,'%f',[4,4])';
R2p=c2r2pr(m+1,n+1);
status = fclose(fid);

elseif c == 3
fid=fopen('c3r1pr.tab','r');
c3r1pr=fscanf(fid,'%f',[4,4])';
R1p=c3r1pr(m+1,n+1);
status = fclose(fid);

fid=fopen('c3r2pr.tab','r');
c3r2pr=fscanf(fid,'%f',[4,4])';
R2p=c3r2pr(m+1,n+1);
status = fclose(fid);

elseif c == 4
fid=fopen('c4r1pr.tab','r');
c4r1pr=fscanf(fid,'%f',[4,4])';
R1p=c4r1pr(m+1,n+1);
status = fclose(fid);

fid=fopen('c4r2pr.tab','r');
c4r2pr=fscanf(fid,'%f',[4,4])';
R2p=c4r2pr(m+1,n+1);
status = fclose(fid);

elseif c == 5
fid=fopen('c5r1pr.tab','r');
c5r1pr=fscanf(fid,'%f',[4,4])';
R1p=c5r1pr(m+1,n+1);
status = fclose(fid);

fid=fopen('c5r2pr.tab','r');
c5r2pr=fscanf(fid,'%f',[4,4])';
R2p=c5r2pr(m+1,n+1);
status = fclose(fid);
```

```
else
  error('c out of range.  Must be integer 1 through 5.')
end

R3prime = R1p + i*R2p;
```

S_ANGLE.M

```
function S = s_angle(m,n,c,p_arg)
%
% The function s_angle returns the value of the angular
% spheroidal wave function for a given m, n, c, and
% p_arg.
%
% Syntex:
%          s_angle(m,n,c,p_arg)
% where:
%      m = degree of spheroidal wave function
%      n = order of spheroidal wave function
%      c = Independent variable c=1/2*k*d
%      p_arg = argument of the Associated Legendre Function,
%              generally eta or cos(zeta)
%
%
% Taken from the book Spheroidal Wave Functions, by
% Carson Flammer, Stanford University Press, 1957
%
% Produced in process of completion of masters thesis,
% Department of General Engineering, San Jose State University
% MATLAB function (c) Richard W. Novy, 1997
%
%
if rem(n-m,2) == 0
  stemp = 0;
  for r = 0:2:8
    tempP = legendre(m+r,p_arg);
    P = tempP(m+1);  % To account for MATLAB indexing starting at 1 not 0.
    clear tempP;
    d = lookup(m,n,r,c);
    stemp = stemp + d*P;
  end
elseif rem(n-m,2) == 1
  stemp = 0;
  for r = 1:2:9
    tempP = legendre(m+r,p_arg);
    P = tempP(m+1);  % To account for MATLAB indexing starting at 1 not 0.
    clear tempP;
    d = lookup(m,n,r,c);
    stemp = stemp + d*P;
```

```
  end
else
  error('m and n must be integers');
end

S = stemp;   % Return answer angular S evaluated at p_arg
```

LOOKUP.M

```
function [d] = lookup(m,n,r,c)
%
% This function performs a look-up table operation
% to find the spheroidal wave function Fourier
% coefficients.
%
% Syntex:
%          d = lookup(m,n,r,c)
%
% where:
%    m = degree of spheroidal wave function
%    n = order of spheroidal wave function
%    r = iteration of summation calling this function
%        r = 0,1,2,3
%    c = Independent variable c=1/2*k*d  Currently this routine
%        is limited to integer c values between 1 and 5.
%
% Tables taken from the book Spheroidal Wave Functions, by
% Carson Flammer, Stanford University Press, 1957
%
% Produced in process of completion of masters thesis,
% Department of General Engineering, San Jose State University
% MATLAB function (c) Richard W. Novy, 1997
%
%
%

if c == 1

 if r==0 | r==1
  fid=fopen('c1r0r1.tab','r');
  c1r0r1=fscanf(fid,'%f',[4,4])';
  d=c1r0r1(m+1,n+1);
  status = fclose(fid);
 elseif r==2 | r==3
  fid=fopen('c1r2r3.tab','r');
  c1r2r3=fscanf(fid,'%f',[4,4])';
  d=c1r2r3(m+1,n+1);
  status = fclose(fid);
 elseif r==4 | r == 5
  fid=fopen('c1r4r5.tab','r');
```

```
    c1r4r5=fscanf(fid,'%f',[4,4])';
    d=c1r4r5(m+1,n+1);
    status = fclose(fid);
  elseif r==6 | r == 7
    fid=fopen('c1r6r7.tab','r');
    c1r6r7=fscanf(fid,'%f',[4,4])';
    d=c1r6r7(m+1,n+1);
    status = fclose(fid);
  elseif r==8 | r == 9
    fid=fopen('c1r8r9.tab','r');
    c1r8r9=fscanf(fid,'%f',[4,4])';
    d=c1r8r9(m+1,n+1);
    status = fclose(fid);
  else
    error('r out of range.  Must be integer 0 through 9');
  end

elseif c == 2

  if r==0 | r==1
    fid=fopen('c2r0r1.tab','r');
    c2r0r1=fscanf(fid,'%f',[4,4])';
    d=c2r0r1(m+1,n+1);
    status = fclose(fid);
  elseif r==2 | r==3
    fid=fopen('c2r2r3.tab','r');
    c2r2r3=fscanf(fid,'%f',[4,4])';
    d=c2r2r3(m+1,n+1);
    status = fclose(fid);
  elseif r==4 | r == 5
    fid=fopen('c2r4r5.tab','r');
    c2r4r5=fscanf(fid,'%f',[4,4])';
    d=c2r4r5(m+1,n+1);
    status = fclose(fid);
  elseif r==6 | r == 7
    fid=fopen('c2r6r7.tab','r');
    c2r6r7=fscanf(fid,'%f',[4,4])';
    d=c2r6r7(m+1,n+1);
    status = fclose(fid);
  elseif r==8 | r == 9
    fid=fopen('c2r8r9.tab','r');
    c2r8r9=fscanf(fid,'%f',[4,4])';
    d=c2r8r9(m+1,n+1);
```

```
        status = fclose(fid);
      else
        error('r out of range.  Must be integer 0 through 9');
      end

  elseif c == 3

    if r==0 | r==1
      fid=fopen('c3r0r1.tab','r');
      c3r0r1=fscanf(fid,'%f',[4,4])';
      d=c3r0r1(m+1,n+1);
      status = fclose(fid);
    elseif r==2 | r==3
      fid=fopen('c3r2r3.tab','r');
      c3r2r3=fscanf(fid,'%f',[4,4])';
      d=c3r2r3(m+1,n+1);
      status = fclose(fid);
    elseif r==4 | r == 5
      fid=fopen('c3r4r5.tab','r');
      c3r4r5=fscanf(fid,'%f',[4,4])';
      d=c3r4r5(m+1,n+1);
      status = fclose(fid);
    elseif r==6 | r == 7
      fid=fopen('c3r6r7.tab','r');
      c3r6r7=fscanf(fid,'%f',[4,4])';
      d=c3r6r7(m+1,n+1);
      status = fclose(fid);
    elseif r==8 | r == 9
      fid=fopen('c3r8r9.tab','r');
      c3r8r9=fscanf(fid,'%f',[4,4])';
      d=c3r8r9(m+1,n+1);
      status = fclose(fid);
    else
      error('r out of range.  Must be integer 0 through 9');
    end

  elseif c == 4
    if r==0 | r==1
      fid=fopen('c4r0r1.tab','r');
      c4r0r1=fscanf(fid,'%f',[4,4])';
      d=c4r0r1(m+1,n+1);
      status = fclose(fid);
    elseif r==2 | r==3
```

```
    fid=fopen('c4r2r3.tab','r');
    c4r2r3=fscanf(fid,'%f',[4,4])';
    d=c4r2r3(m+1,n+1);
    status = fclose(fid);
  elseif r==4 | r == 5
    fid=fopen('c4r4r5.tab','r');
    c4r4r5=fscanf(fid,'%f',[4,4])';
    d=c4r4r5(m+1,n+1);
    status = fclose(fid);
  elseif r==6 | r == 7
    fid=fopen('c4r6r7.tab','r');
    c4r6r7=fscanf(fid,'%f',[4,4])';
    d=c4r6r7(m+1,n+1);
    status = fclose(fid);
  elseif r==8 | r == 9
    fid=fopen('c4r8r9.tab','r');
    c4r8r9=fscanf(fid,'%f',[4,4])';
    d=c4r8r9(m+1,n+1);
    status = fclose(fid);
  else
    error('r out of range.  Must be integer 0 through 9');
  end


elseif c == 5

  if r==0 | r==1
    fid=fopen('c5r0r1.tab','r');
    c5r0r1=fscanf(fid,'%f',[4,4])';
    d=c5r0r1(m+1,n+1);
    status = fclose(fid);
  elseif r==2 | r==3
    fid=fopen('c5r2r3.tab','r');
    c5r2r3=fscanf(fid,'%f',[4,4])';
    d=c5r2r3(m+1,n+1);
    status = fclose(fid);
  elseif r==4 | r == 5
    fid=fopen('c5r4r5.tab','r');
    c5r4r5=fscanf(fid,'%f',[4,4])';
    d=c5r4r5(m+1,n+1);
    status = fclose(fid);
  elseif r==6 | r == 7
    fid=fopen('c5r6r7.tab','r');
```

```
    c5r6r7=fscanf(fid,'%f',[4,4])';
    d=c5r6r7(m+1,n+1);
    status = fclose(fid);
  elseif r==8 | r == 9
    fid=fopen('c5r8r9.tab','r');
    c5r8r9=fscanf(fid,'%f',[4,4])';
    d=c5r8r9(m+1,n+1);
    status = fclose(fid);
  else
    error('r out of range.  Must be integer 0 through 9');
  end

else
  error('c out of range.  Must be integer 1 through 5.');
end
```

APPENDIX C - LOOKUP TABLES

TABLES FOR d COEFFICIENTS

C1R0R1.TAB

.94837e0	.94217e0	.22044e-1	.17108e-1
0	.98074e0	.97013e0	.33693e-1
0	0	.99022e0	.98179e0
0	0	0	.99392e0

C1R2R3.TAB

-.10195e0	-.38007e-1	.10251e1	.98941e0
0	-.12734e-1	-.11833e-1	.100905e1
0	0	-.39671e-2	-.51649e-2
0	0	0	-.17299e-2

C1R4R5.TAB

.17316e-2	.43231e-3	-.25156e-1	-.17461e-1
0	.85735e-4	.66284e-4	-.10667e-1
0	0	.13242e-4	.16368e-4
0	0	0	.32762e-5

C1R6R7.TAB

-.12439e-4	-.23553e-5	.21193e-3	.11659e-3
0	-.33126e-6	-.21608e-6	.50833e-4
0	0	-.30713e-7	-.34497e-7
0	0	0	-.49200e-8

C1R8R9.TAB

.49490e-7	.75651e-8	-.92262e-6	-.42212e-6
0	.82303e-9	.46283e-9	-.14307e-6
0	0	0	0
0	0	0	.57374e-11

C2R0R1.TAB

.83162e0	.79276e0	.83921e-1	.67686e-1
0	.93070101	.88878e0	.12739448
0	0	.96260	.93072
0	0	0	.97672

C2R2R3.TAB

-.32059	-.13049	.10845e1	.95749
0	-.44714640e-1	-.42790e-1	.10293799e1
0	0	-.14622e-1	-.19242e-1
0	0	0	-.65420e-2

C2R4R5.TAB

.21062e-1	.59797e-2	-.10800	-.67949
0	.11668363e-2	.95266e-3	-.43462124e-1
0	0	.19025e-3	.24160e-3
0	0	0	.48535e-4

C2R6R7.TAB

-.59551e-3	-.13080e-3	.36596e-2	.18186e-2
0	-.17729547e-4	-.12376e-4	.82742033e-3
0	0	.17385e-5	-.20249e-5
0	0	0	-.28777e-6

C2R8R9.TAB

.93876e-5	.16842e-5	-.63916e-4	-.026367e-4
0	.17451722e-6	.10578e-6	-.93072037e-5
0	0	.11441e-7	.12115e-7
0	0	0	.13304e-8

C2R10R11.TAB

-.94371e-7	-.14318e-7	.68648e-6	.24251e-6
0	0	-.64097e-9	.69919976e-7
0	0	0	0
0	0	0	-.48578e-11

C3R0R1.TAB

.71480	.60970	.16387	.14644
0	.86663809	.77681	.25854188
0	0	.92379	.85610
0	0	0	.95107

C3R2R3.TAB

-.51422	-.22885	.11188e1	.90068
0	-.82909539e-1	-.81877e-1	.10421783e1
0	0	-.29016e-1	-.38651e-1
0	0	0	-.13480e-1

C3R4R5.TAB

.71137e-1	.23672e-1	-.26116	-.14678
0	.46155268e-2	.40466e-2	-.99059250e-1
0	0	.81422e-3	.10728e-2
0	0	0	.21748e-3

C3R6R7.TAB

-.43773e-2	-.11665e-2	.20202e-1	.89060e-2
0	-.15321188e-3	-.11734e-3	.42375950e-2
0	0	-.16323e-4	-.20017e-4
0	0	0	-.28394e-5

C3R8R9.TAB

.15220e-3	.33819e-4	-.79994e-3	-.29172e-3
0	.33306131e-5	.22445e-5	-.10712776e-3
0	0	.23767e-6	.26752e-6
0	0	0	.29102e-7

C4R0R1.TAB

.62537	.44886	.22575	.23404
0	.80272	.65807	.39433
0	0	.88015	.76970
0	0	0	.92027

C4R2R3.TAB

-.63356e0	-.29359e0	.10554e1	.80626e0
0	-.11712e0	-.11769e0	.102543e1
0	0	-.44112e-1	-.59007e-1
0	0	0	-.21405e-1

C4R4R5.TAB

.14138e0	.53331e-1	-.46970e0	-.24610e0
0	.10772e-1	.10097e-1	-.17380e0
0	0	.20777e-2	.28417e-2
0	0	0	.58631e-3

C4R6R7.TAB

-.14689e-1	-.46370e-2	.66025e-1	.27035e-1
0	-.60952e-3	-.51308e-3	.13191e-1
0	0	-.44112e-1	-.59007e-1
0	0	0	-.21405e-1

C4R8R9.TAB

.87978e-3	.23780e-3	-.46988e-2	-.15895e-2
0	.22926e-4	.17281e-4	-.59168e-3
0	0	.18073e-5	.21798e-5
0	0	0	.23579e-6

C5R0R1.TAB

.56032	.33290	.25069	.29568
0	.74568	.54991	.50609
0	0	.83650	.68211
0	0	0	.88728

C5R2R3.TAB

-.69561	-.31756	.89072	.66145
0	-.14351	-.14352	.96817
0	0	-.57882	-.77006e-1
0	0	0	-.29361e-1

C5R4R5.TAB

.21548	.86971e-1	.67508e0	-.34845
0	.18863e-1	.18547e-1	-.25706
0	0	.39717e-2	.55988e-2
0	0	0	.11876e-2

C5R6R7.TAB

-.32721e-1	-.11568e-1	.15139e0	.61728e-1
0	-.15808e-2	-.14397e-2	.30334e-1
0	0	-.20429e-3	-.27928e-3
0	0	0	-.40285e-4

C5R8R9.TAB

.29359e-2	.91415e-3	-.16987e-1	-.57625e-2
0	.89688e-4	.74621e-4	-.21167e-2
0	0	.78295e-5	.10096e-4
0	0	0	.10944e-5

Tables For R'

C1R1PR.TAB

-.3422e0	.2357e0	.1283e0	.258e-1
0	.8384e0	.2067e0	.314e-1
0	0	.1389e0	.228e-1
0	0	0	.121e-1

C1R2PR.TAB

.7279e1	.1672e2	.9116e2	.7922e3
0	.2624e2	.1313e3	.1040e4
0	0	.3121e3	.2092e4
0	0	0	.5353e4

C2R1PR.TAB

-.1203e1	-.7400e-2	.3407e0	.1701e0
0	.1356e1	.6840e0	.2197e0
0	0	.5033e0	.1639e0
0	0	0	.906e-1

C2R2PR.TAB

.4772e1	.5900e1	.1290e2	.5307e2
0	.7208e1	.1779e2	.6992e2
0	0	.4025e2	.1398e3
0	0	0	.3468e3

C3R1PR.TAB

-.2260e1	-.8068e0	.2414e0	.3872e0
0	.1373e1	.1107e1	.5816e0
0	0	.9588e0	.4634e0
0	0	0	.2754e0

C3R2PR.TAB

.3762e1	.4238e1	.5410e1	.1208e2
0	.4479e1	.6377e1	.1569e2
0	0	.1260e2	.3038e2
0	0	0	.7222e2

C4R1PR.TAB

-.3233e1	-.1876e1	-.4143e0	.4098e0
0	.8776e0	.1183e1	.9474e0
0	0	.1341e1	.8563e0
0	0	0	.5642e0

C4R2PR.TAB

.2692e1	.3459e1	.3942e1	.5268e1
0	.4056e1	.4086e1	.6153e1
0	0	.5981e1	.1092e2
0	0	0	.2433e2

C5R1PR.TAB

-.3901e1	-.2881e1	-.1460e1	-.635e-1
0	-.258e-1	.7911e0	.1065e1
0	0	.1502e1	.1208e1
0	0	0	.9113e0

C5R2PR.TAB

.1909e1	.2523e1	.3637e1	.3788e1
0	.4022e1	.3713e1	.4543e1
0	0	.4045e1	.5482e1
0	0	0	.1074e2

May 13, 1998

Mr. Richard W. Novy
P.O. Box 64011
Sunnyvale, CA 94088-4011

Dear Mr. Novy:

I am in receipt of your request for permission to use a figure in your master thesis (copy
enclosed). Permission is granted to use this figure on the enclosed for one time at no charge.

We are aware that University Microfilms, Inc. may supply single copies on demand.

Should you have any other questions, please do not hestitate to contact me at anytime.

Thank you.

Sincerely,

Ruth M. Rearick
Permissions Coordinator

/rmr
Enclosure

January 21, 1998

Hemisphere Publishing Corporation
1900 Frost Road; Suite 101
Bristol, PA 19007

Attention: Permissions
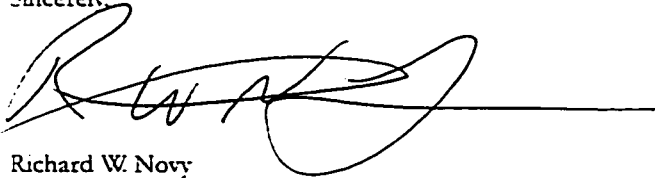
Dear Hemisphere Publishing Corporation,

I would like permission to use a figure in my masters thesis. The figure I am interested in is Figure 11.1: Prolate Spheroidal Geometry, from the book Electromagnetic and Acoustic Scattering by Simple Shapes, by Bowman, Senior, and Uslenghi, ISBN 0-89116-885-0.

I would appreciate a letter expressing the appropriate permission and your preferred line crediting the work.

Thank-you for your assistance.

Sincerely,

Richard W. Novy

IMAGE EVALUATION
TEST TARGET (QA–3)

1.0 2.8 2.5 2.2 2.0 1.8 1.1 1.6 1.25 1.4

3.2 3.6 4.0 4.5 5.0

150mm

6"
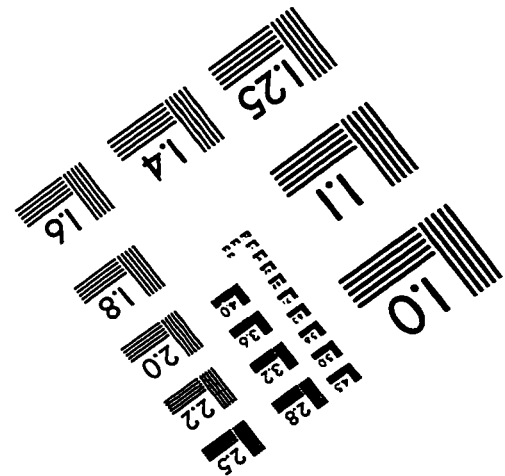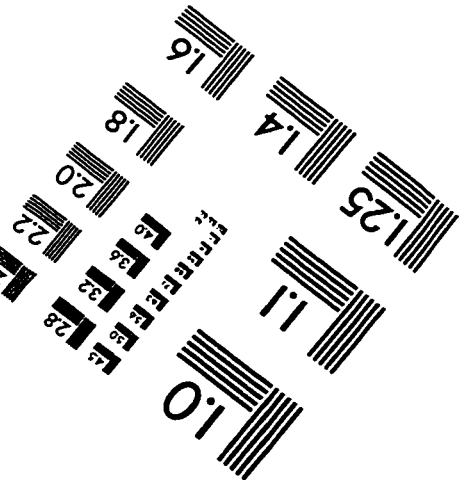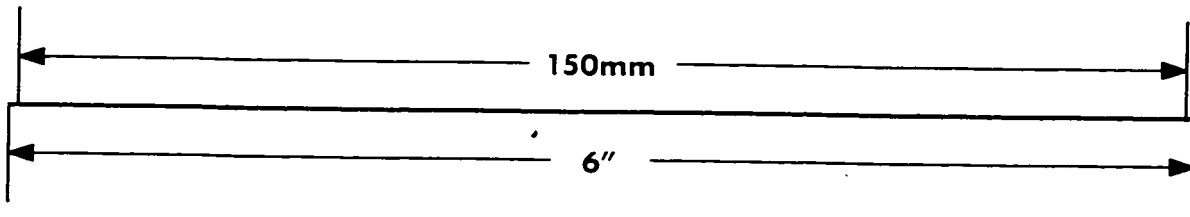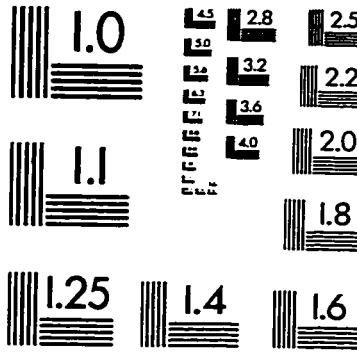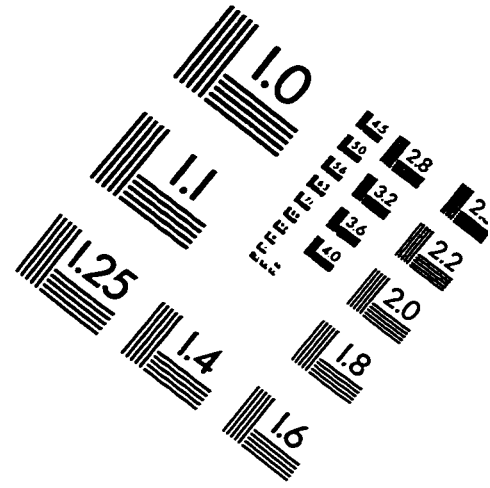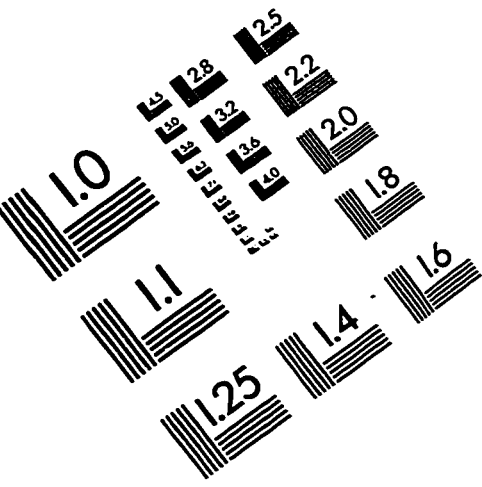
APPLIED IMAGE . Inc
1653 East Main Street
Rochester, NY 14609 USA
Phone: 716/482-0300
Fax: 716/288-5989